Supplementary Information

Controlling Singlet Fission with Coordination Chemistry-Induced Structural Perturbations in a Series of Dipyridyl Pyrrole Bipentacenes

Ryan D. Ribson[1], Gyeongshin Choi[1], Ryan G. Hadt[1]*, Theodor Agapie[1]*

[1]Division of Chemistry and Chemical Engineering, Arthur Amos Noyes Laboratory of Chemical Physics, California Institute of Technology, Pasadena, California 91125, United States

*Corresponding authors: rghadt@caltech.edu, agapie@caltech.edu

I. Experimental Considerations

General Information

Air- and moisture-sensitive compounds were handled with standard Schlenk line techniques or in a $N_{2(g)}$ atmosphere glove box. When air- and moisture-free techniques were required, dry solvents were acquired from an alumina solvent still. No unexpected or unusually high safety hazards were encountered. 2,6-dibromopyridine was purchased from Combi-Blocks Inc. and used without further purification. Tin (II) dichloride dihydrate was purchased from Matrix Scientific and used without further purification. $Pd(PPh_3)_4$ was purchased from Oakwood Chemicals, stored under inert atmosphere, and used without further purification. Lithium hexamethyldisilazide and potassium hexamethyl disilazide were purchased from Sigma Aldrich, stored in an inert atmosphere glovebox, and used without further purification. 13-hydroxy-13-[(triisopropylsilyl)ethynyl]pentacen-6(13H)-one (Ketone 1, Figure S1)[1] and 2,5-bis(pinacolatoboranyl)pyrrole[2] were synthesized according to previous reports. ^{1}H, ^{13}C, and 2D NMR spectra were collected on a 400 MHz Varian spectrometer. All pentacene solution-state samples for optical spectroscopy were prepared in an inert-atmosphere glovebox using solvents dried and purified on an alumina drying column and degassed prior to being brought into the glovebox. Steady state absorption spectra were collected using a Varian Cary 500 Scan spectrophotometer. Glotaran (http://glotaran.org), a user interface for the R-based time-resolved fitting software TIMP, was used for kinetic modelling of the transient absorption data.[3]

II. Synthetic Procedures

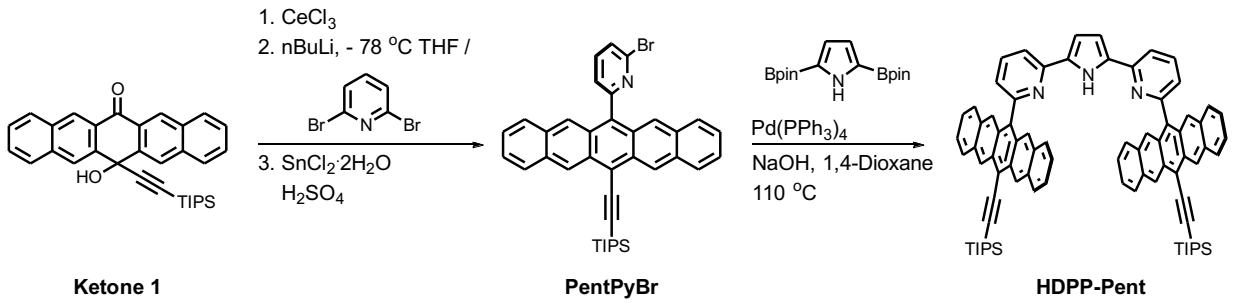

Figure S1. Synthetic scheme for HDPP-Pent. Ketone 1 is activated with $CeCl_3$ then converted into PentPyBr by deprotonation and nucleophilic attack by monolithiated 2,6-dibromopyridine at -78 °C, followed by reductive aromatization with $SnCl_2 \cdot 2H_2O$. HDPP-Pent is then furnished after a double-Suzuki-Miyaura coupling of PentPyBr with 2,5-bis(pinacolatoboranyl)pyrrole using catalytic $Pd(PPh_3)_4$.

Synthesis of PentPyBr

Ketone 1 (10 mmol) was dissolved in THF in an oven-dried flask under inert conditions. $CeCl_3$ (20 mmol) was added under positive $N_{2(g)}$ pressure and the mixture was stirred for 1 h at room temperature. In a separate flask under nitrogen atmosphere, dibromopyridine (30 mmol) was dissolved in THF and cooled to -78 °C. nBuLi (1.6M solution in hexanes, 30 mmol) was then added slowly to the pyridine solution, which was stirred for 30 min to achieve monolithiation. The solution of Ketone 1 was cooled to -78 °C and the lithiated pyridine solution was slowly cannula transferred under positive nitrogen pressure with stirring. The mixture was warmed to room temperature and stirred for 15 h. Aqueous ammonium chloride solution was slowly added to quench. The brown solution was filtered through a pad of celite to remove salts. The organics were taken up in dichloromethane and washed with brine (2x), dried over Mg_2SO_4, and concentrated to an oily solid. This material was taken up in THF (80 mL) and transferred to a three neck roundbottom flask. The solution was sparged with $N_{2(g)}$ and $SnCl_2 \cdot 2H_2O$ (20 mmol) was added followed by slow addition of 10% H_2SO_4 (3 mL). The solution was sparged again and stirred for 3 h under nitrogen atmosphere at room temperature. The reaction was neutralized with $K_2CO_{3(aq)}$ and the reaction mixture was filtered through celite. The product was extracted with dichloromethane and dried over Mg_2SO_4. The mixture was concentrated, and the target compound was crashed from methanol to give a dark blue powder. ^{1}H NMR (400 MHz, $CDCl_3$, 25 ºC): δ 9.37 (s, 2H), 8.16 (s, 2H), 7.96 (d, J = 8.5 Hz, 2H), 7.93 – 7.89 (m, 1H), 7.81 (dd, J = 8.0, 1.0 Hz, 1H), 7.77 (d, J = 8.5 Hz, 2H), 7.60 (dd, J = 7.4, 1.0 Hz, 1H), 7.40 – 7.29 (m, 5H), 1.39 (s, 21H). ^{13}C NMR (101 MHz, $CDCl_3$, 25 ºC): δ 159.7, 142.7, 139.0, 134.0, 132.0, 130.9, 128.8, 128.7, 128.3, 127.5, 126.5, 126.2, 126.1, 125.9, 125.1, 119.2, 106.4, 104.7, 19.2, 11.8. HRMS (FAB+) Calcd. For $C_{38}H_{36}NSiBr$: 615.1780. Found: 615.1770.

Synthesis of HDPP-Pent

PentPyBr (2.5 g), 2,5-bis(pinacolatoboranyl)pyrrole (0.65 mg), and NaOH (8.7 mg) were added to an oven-dried Schlenk flask under nitrogen atmosphere and a degassed 9:1 1,4-dioxane/H_2O solution (100 mL) was added. $Pd(PPh_3)_4$ (5 mol%) was added under a counter-flow of $N_{2(g)}$ and the reaction mixture was heated to 110 °C for 5 h. Volatiles were removed under vacuum pressure and the organics were taken up in dichloromethane, washed with brine (2x), dried over Mg_2SO_4, filtered, and concentrated to dryness. HDPP-Pent was obtained as a blue solid by silica-column chromatography (3 : 1 Hexanes/CH_2Cl_2, followed by 5 : 1 Hexanes/THF, then 5:1:1 Hexanes/CH_2Cl_2/Toluene with 1% MeOH). ^{1}H NMR (400 MHz, CD_2Cl_2, 25 ºC): δ 10.39 (s, 1H), 8.48 (br s, 4H), 7.64 – 7.58 (m, 5H), 7.48 (d, 5H), 7.43 (br s, 4H), 7.07 (d, 2H), 6.95 (dd, J = 6.2, 2.1 Hz, 2H), 6.84 – 6.73 (m, 9H), 1.46 (br s, 42H). ^{13}C NMR (101 MHz, CD_2Cl_2, 25 ºC): δ 158.1, 149.7, 136.0, 135.8, 133.3, 130.7, 130.0, 129.6, 127.7, 127.2, 127.0, 125.0, 124.6, 124.5, 124.0, 123.6, 117.2, 116.9, 109.3, 105.4, 103.4, 19.3, 12.0.

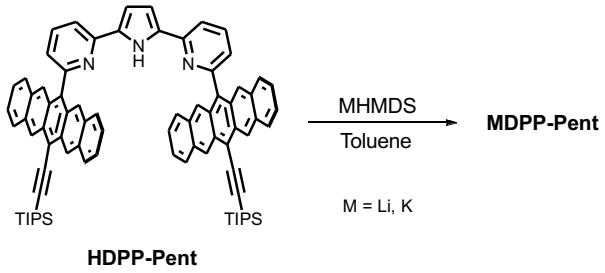

Figure S2. Synthetic scheme for MDPP-Pent (M = Li, K). HDPP-Pent is deprotonated with the appropriate alkali metal hexamethyldisilazide (MHMDS).

Synthesis of Li_2(DPP-Pent)$_2$

HDPP-Pent (0.1 mmol) was dissolved in toluene (3 mL) and a solution of lithium hexamethyldisilazide (0.1 mmol) in toluene (2 mL) was added and the mixture was stirred for 20 min. The solution quickly turned from blue to blue-green. Volatiles were removed via vacuum pressure and the desired product was obtained as a blue-green powder. ^{1}H NMR (400 MHz, CD_2Cl_2, 25 °C): δ 9.10 (s, 4H), δ 7.84 (d, 4H), δ 7.75 (s, 4H), δ 7.51 (d, 4H), δ 7.23 (dd, 4H), δ 6.93 (dd, 4H), δ 6.04 (m, 4H), δ 5.12 (d, 2H), δ 4.36 (s, 2H), δ 1.53 (m, 42H).

Synthesis of KDPP-Pent

HDPP-Pent (0.1 mmol) was dissolved in toluene (3 mL) and a solution of potassium hexamethyldisilazide (0.1 mmol) in toluene (2 mL) was added and the mixture was stirred for 20 min. The solution quickly turned from blue to blue-green. Volatiles were removed via vacuum pressure and the desired product was obtained as a blue-green powder. ^{1}H NMR (400 MHz, CD_2Cl_2, 25 °C): δ 9.13 (s, 4H), δ 8.15 (s, 4H), δ 7.80 (m, 8H), δ 7.59 (d, 4H), δ 7.24 (m, 4H), δ 7.15 (m, 4H), δ 7.01 (s, 2H), δ 6.96 (d, 2H), δ 1.35 (m, 42H).

Synthesis of NaDPP-Pent

HDPP-Pent (0.1 mmol) was dissolved in toluene (3 mL) and a solution of sodium hexamethyldisilazide (0.1 mmol) in toluene (2 mL) was added and the mixture was stirred for 20 min. The solution quickly turned from blue to blue-green. Volatiles were removed via vacuum pressure and the desired product was obtained as a blue-green powder. ^{1}H NMR (400 MHz, CD_2Cl_2, 25 °C): δ 9.07 (s, 4H), δ 8.09 (s, 4H), δ 7.79 (m, 8H), δ 7.59 (d, 4H), δ 7.24 (m, 4H), δ 7.15 (m, 4H), δ 7.04 (s, 2H), δ 6.94 (d, 2H), δ 1.36 (m, 42H).

III. 2D Rotating Frame Overhauser Effect Spectroscopy (ROESY)

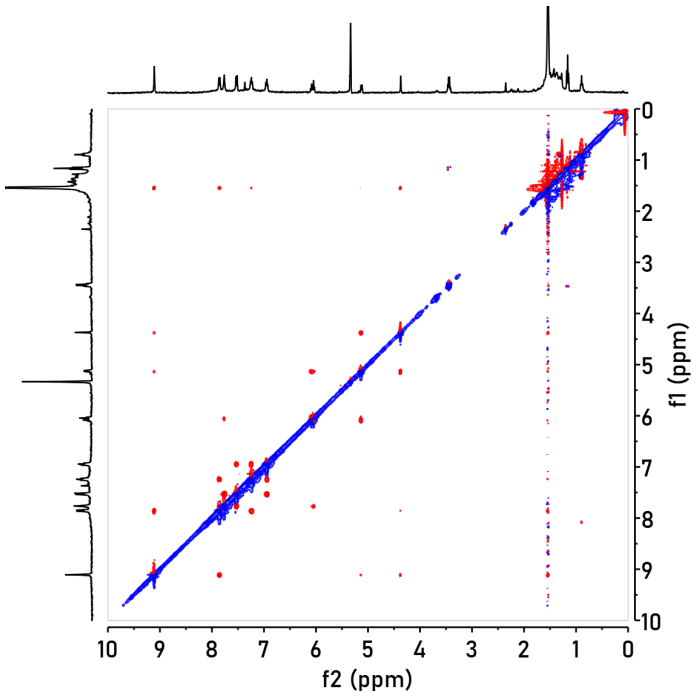

Figure S3. 2D ROESY spectrum of $Li_2(DPP\text{-}Pent)_2$ (400 MHz, CD_2Cl_2).

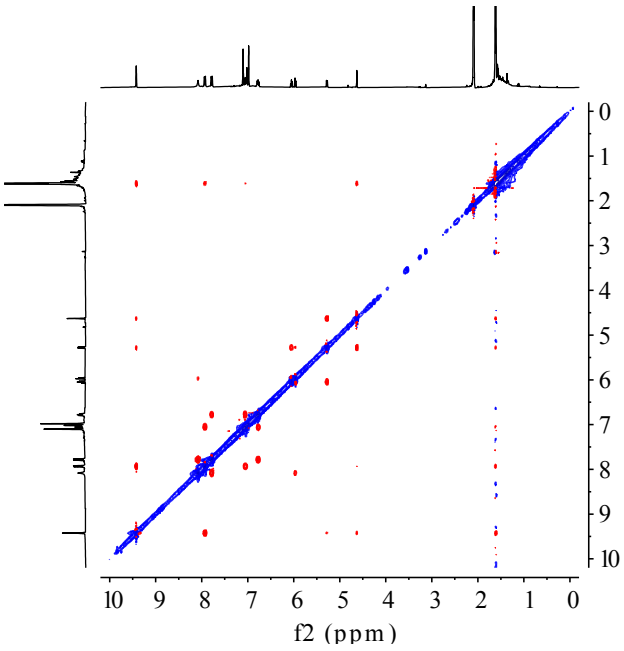

Figure S4. 2D ROESY spectrum of $Li_2(DPP\text{-}Pent)_2$ (400 MHz, toluene-d8).

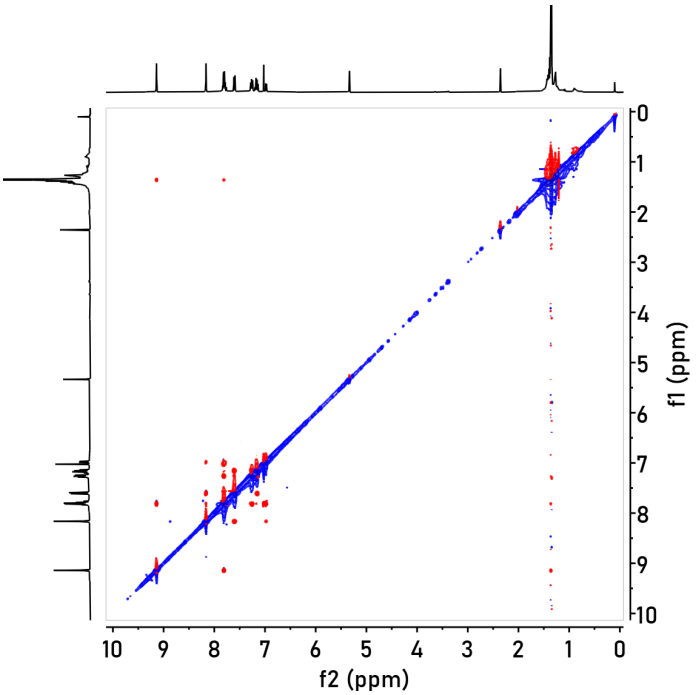

Figure S5. 2D ROESY spectrum of KDPP-Pent (400 MHz, CD_2Cl_2).

IV. Steady-state Absorption and Emission Spectroscopy

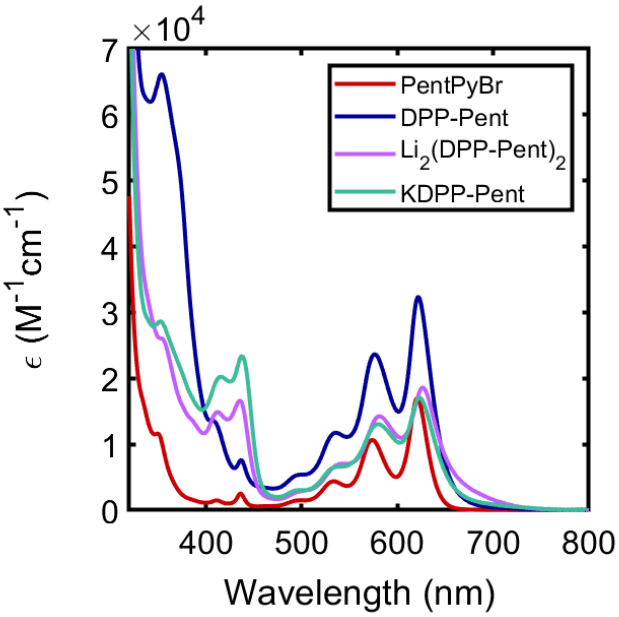

Figure S6. Visible absorption spectra of PentPyBr (red), HDPP-Pent (blue), $Li_2(DPP\text{-}Pent)_2$ (purple), and KDPP-Pent (teal) in toluene.

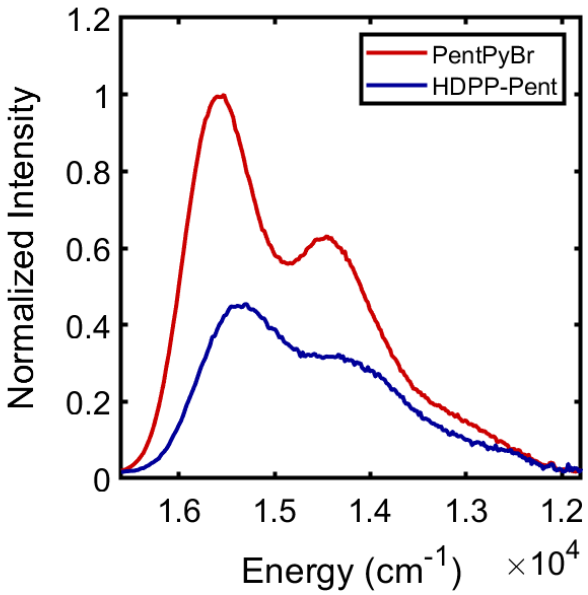

Figure S7. Emission spectra of PentPyBr (red) and HDPP-Pent (blue). The PentPyBr maximum signal intensity was normalized to one and the HDPP-Pent spectrum was scaled such that the integrated intensity of the samples reflected their relative estimated quantum yields.

V. Time-Resolved Luminescence Spectroscopy

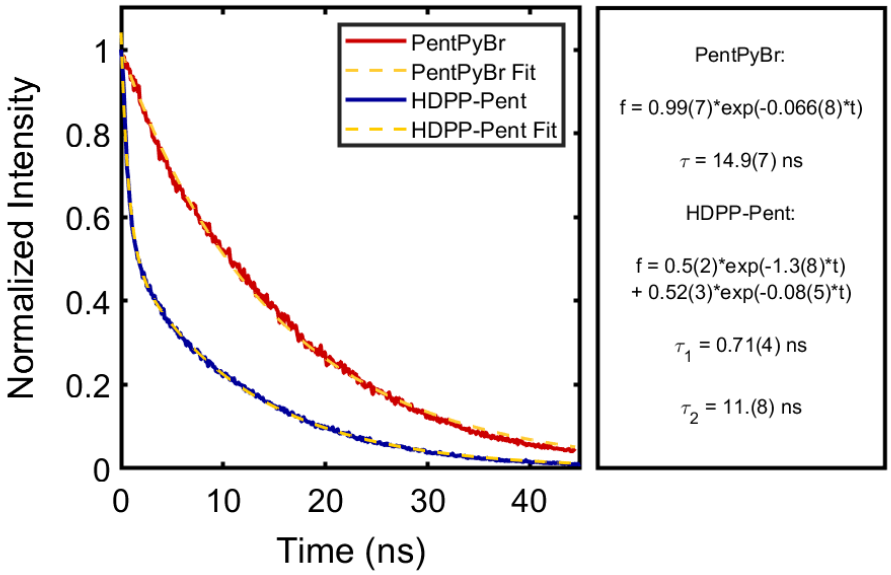

Figure S8. Time-resolved luminescence spectra of PentPyBr (λ_{obs} = 640 nm) and HDPP-Pent (λ_{obs} = 650 nm) after excitation at 532 nm. The spectra were normalized to a maximum of 1. The fluorescence decay of PentPyBr was fit to a monoexponential function (τ = 15 ns), whereas the decay of HDPP-Pent had to be fit biexponentially (τ_1 = 0.71 ns, τ_2 = 11.8 ns).

VI. Transient Absorption Spectroscopy

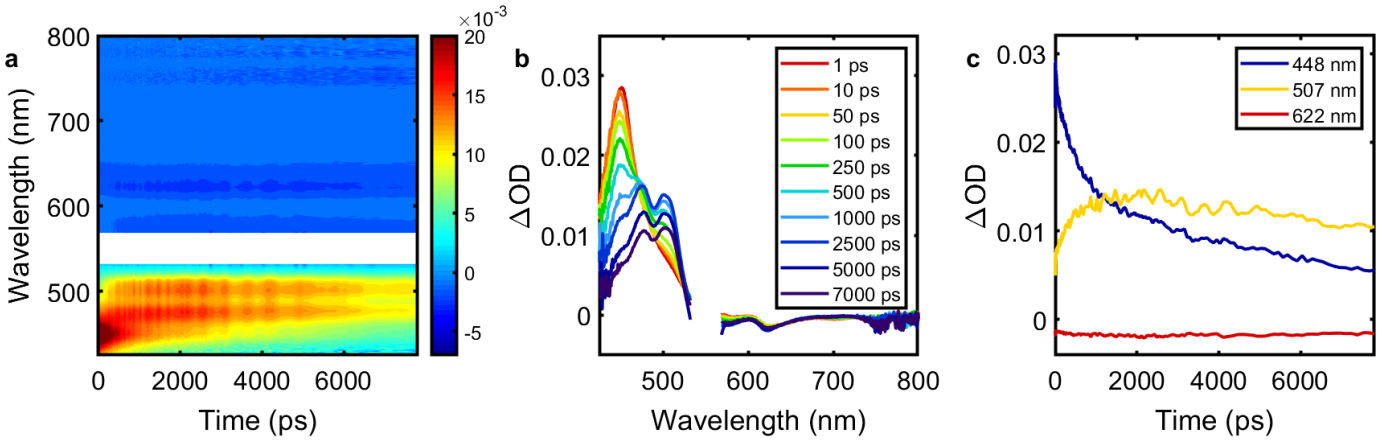

Figure S9. Femtosecond visible transient absorption spectra of HDPP-Pent (50 μM, toluene) after excitation at 550 nm (0.100 μJ/pulse): (a) contour plot, (b) spectral traces at various time delays, (c) selected time traces at 448, 507, and 622 nm.

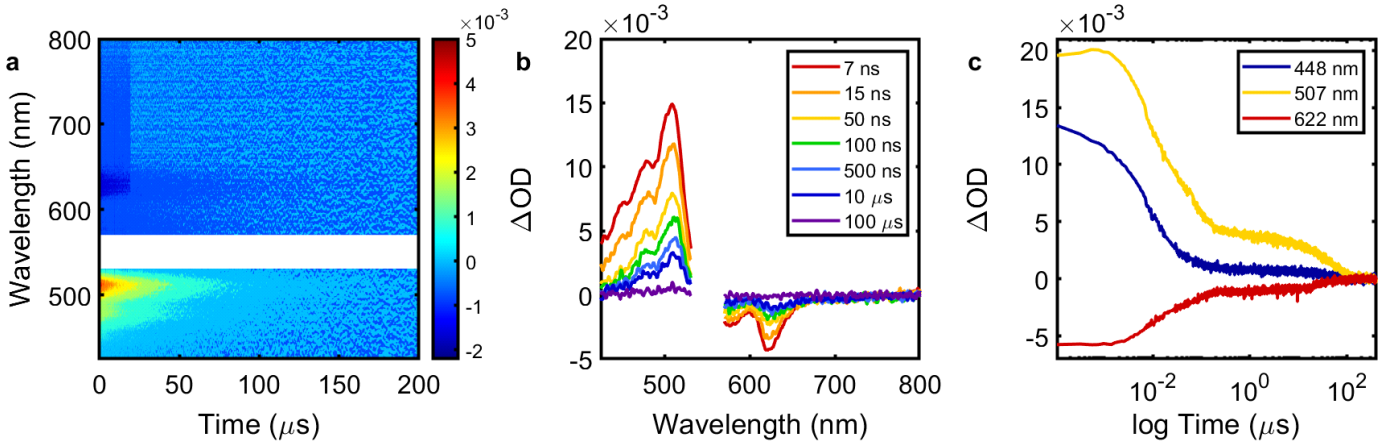

Figure S10. Nanosecond visible transient absorption spectra of HDPP-Pent (50 μM, toluene) after excitation at 550 nm (0.100 μJ/pulse): (a) contour plot, (b) spectral traces at various time delays, (c) selected time traces at 448, 507, and 622 nm.

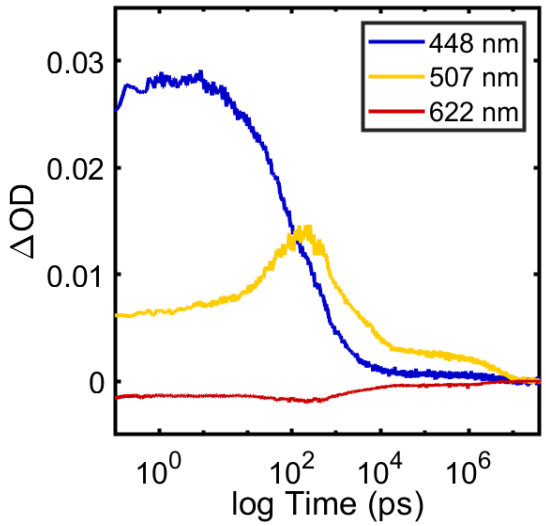

Figure S11. Combined visible fs and ns TA spectra of HDPP-Pent (50 μM, toluene) after excitation at 550 nm (0.100 μJ/pulse); time traces selected at 448, 507, and 622 nm.

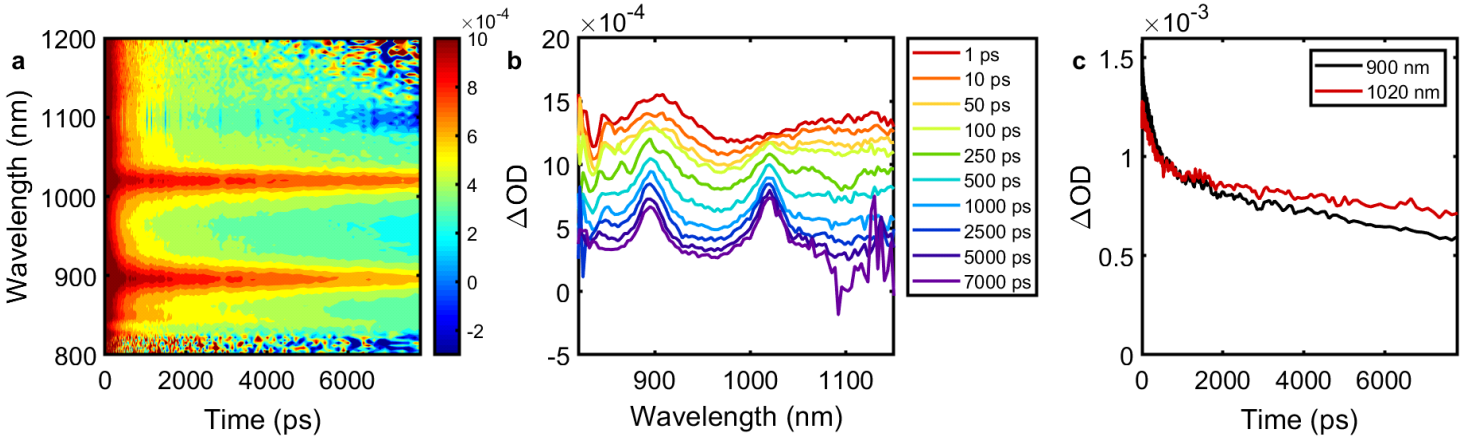

Figure S12. Near-IR fsTA spectra of HDPP-Pent (50 μM, toluene) after excitation at 550 nm (0.100 μJ/pulse): (a) contour plot, (b) spectral traces at various time delays, (c) selected time traces at 900 and 1020 nm.

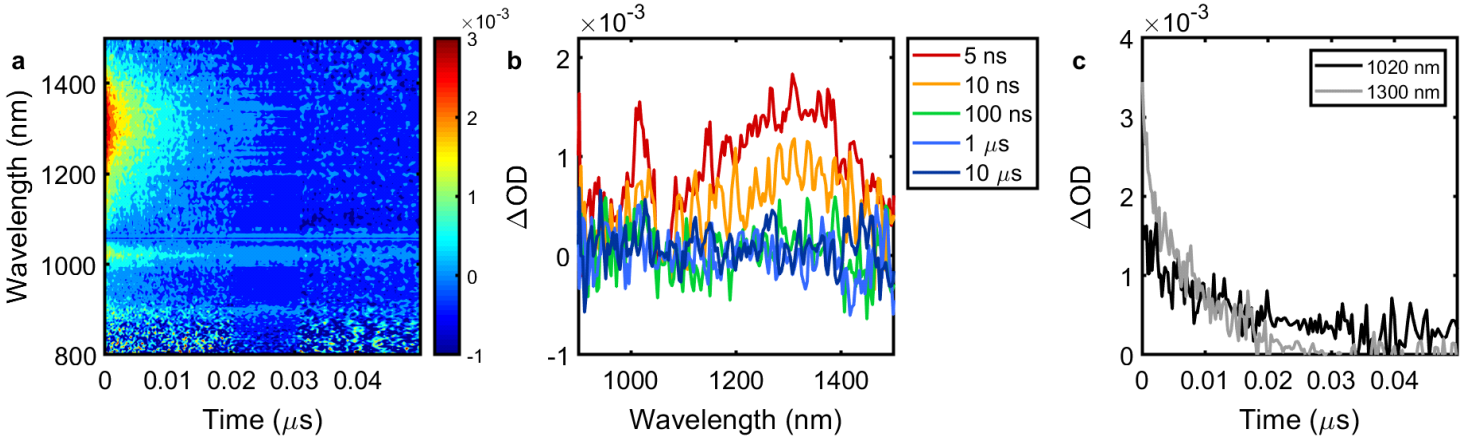

Figure S13. Near-IR nsTA spectra of HDPP-Pent (50 μM, toluene) after excitation at 550 nm (0.100 μJ/pulse): (a) contour plot, (b) spectral traces at various time delays, (c) selected time traces at 900 and 1020 nm.

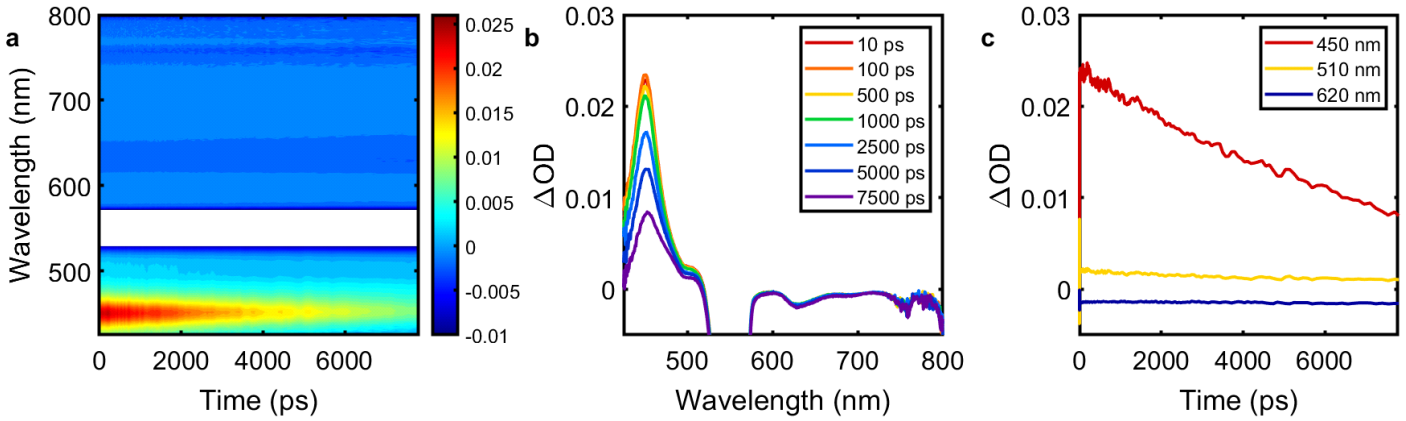

Figure S14. Visible fsTA spectra of PentPyBr (80 µM, toluene) after excitation at 550 nm (0.100 µJ/pulse): (a) contour plot, (b) spectral traces at various time delays, (c) selected time traces at 900 and 1020 nm.

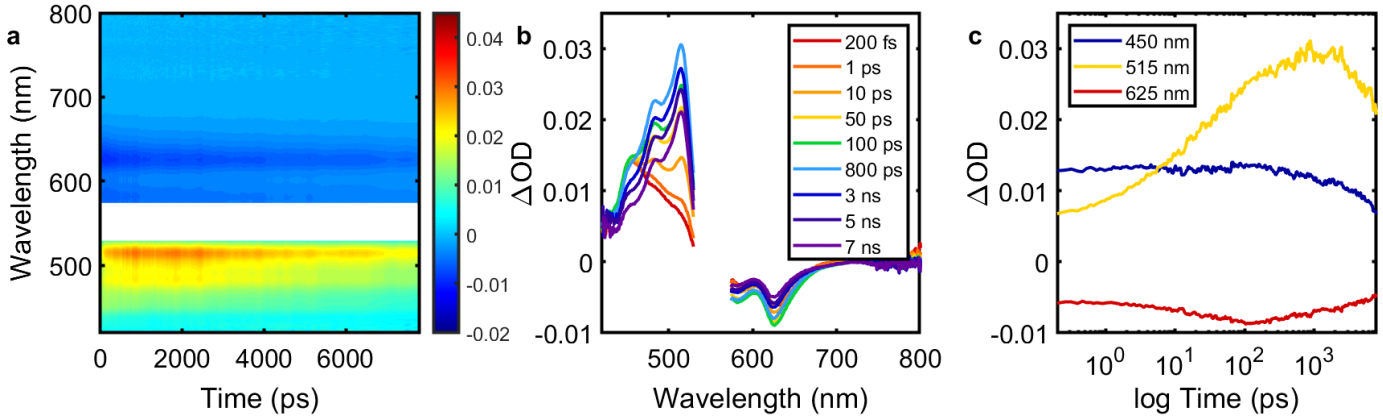

Figure S15. Visible fsTA spectra of Li_2(DPP-Pent)$_2$ (50 μM, toluene) after excitation at 550 nm (0.100 μJ/pulse): (a) contour plot, (b) spectral traces at various time delays, (c) selected time traces at 450, 515, and 625 nm.

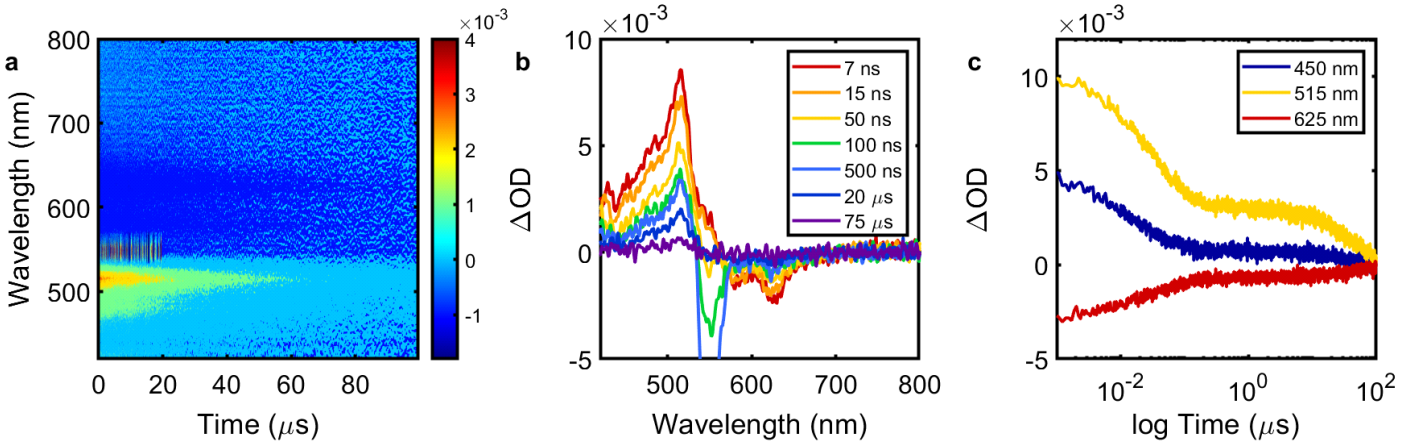

Figure S16. Visible nsTA spectra of Li_2(DPP-Pent)$_2$ (50 μM, toluene) after excitation at 550 nm (0.100 μJ/pulse): (a) contour plot, (b) spectral traces at various time delays, (c) selected time traces at 450, 515, and 625 nm.

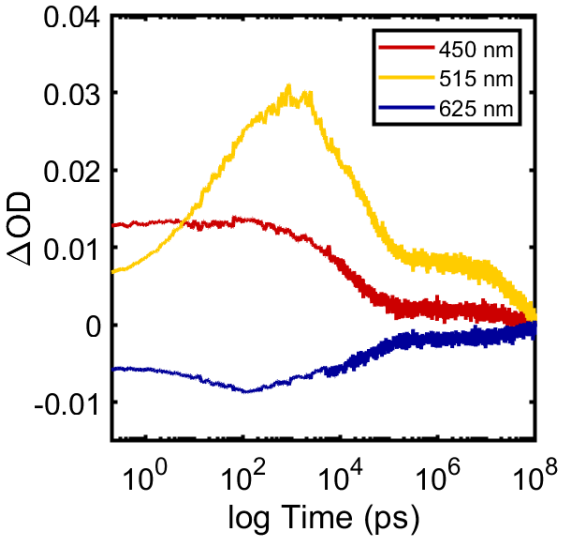

Figure S17. Combined visible fs and ns TA spectra of $Li_2(DPP\text{-}Pent)_2$ (50 μM, toluene) after excitation at 550 nm (0.100 μJ/pulse); time traces selected at 450, 515, and 625 nm.

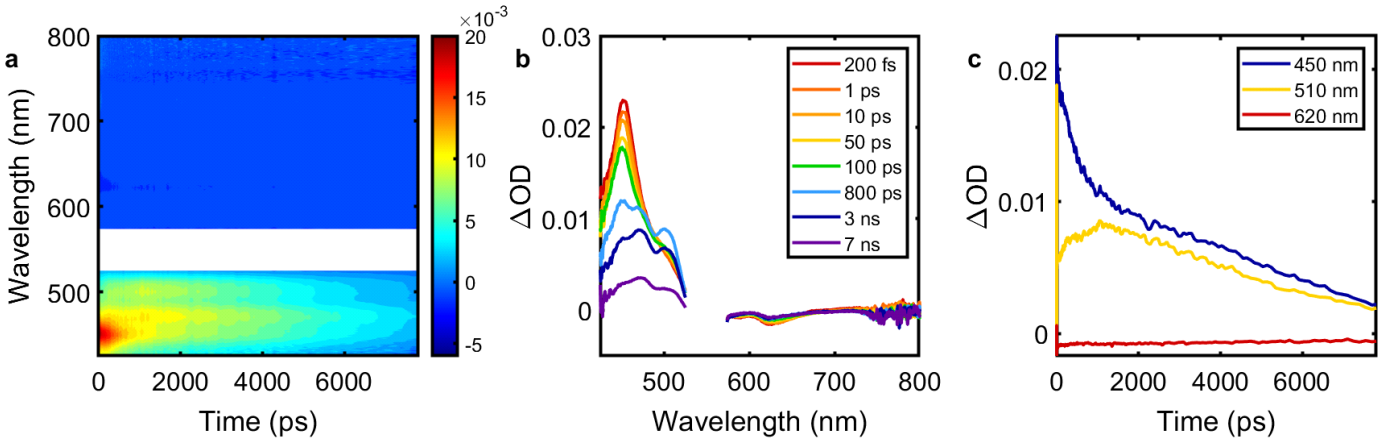

Figure S18. Visible fsTA spectra of KDPP-Pent (50 µM, toluene) after excitation at 550 nm (0.100 µJ/pulse): (a) contour plot, (b) spectral traces at various time delays, (c) selected time traces at 450, 510, and 620 nm.

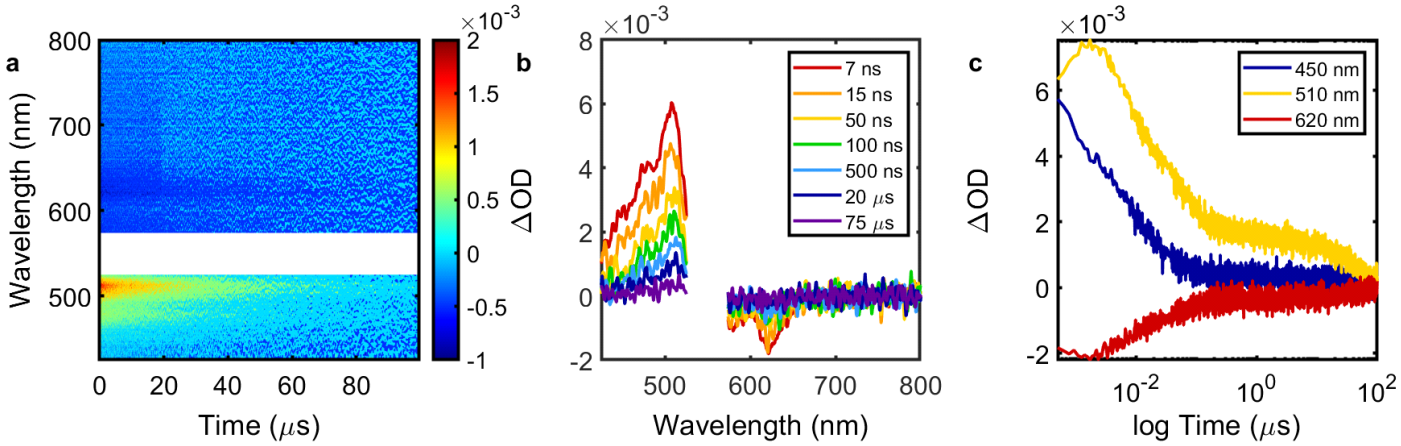

Figure S19. Visible nsTA spectra of KDPP-Pent (50 μM, toluene) after excitation at 550 nm (0.100 μJ/pulse): (a) contour plot, (b) spectral traces at various time delays, (c) selected time traces at 450, 510, and 620 nm.

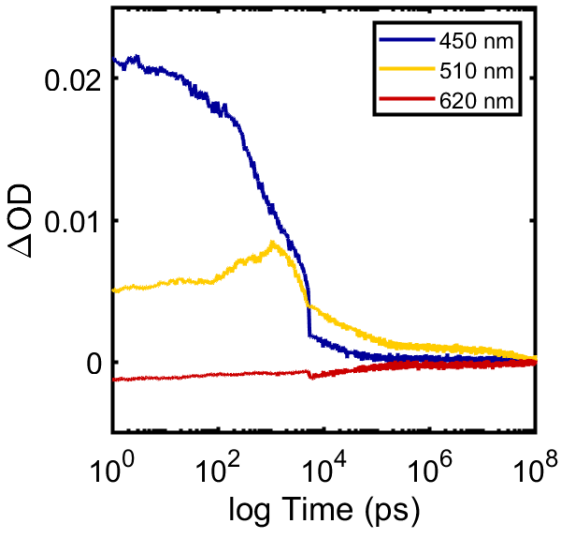

Figure S20. Combined visible fs and ns TA spectra of KDPP-Pent (50 μM, toluene) after excitation at 550 nm (0.100 μJ/pulse); time traces selected at 450, 510, and 620 nm.

VII. Target Kinetic Analysis

HDPP-Pent

For HDPP-Pent, the time-resolved luminescence data provide information solely on the dynamics of the S_1 state independent of the TA spectroscopy. The results of the emission experiment may therefore be appropriately applied to a kinetic model for fitting the composite TA data. Our model assumes the decay of the ^{1}ESA feature should mirror the biexponential decay observed in the time-resolved emission data, as both reflect the dynamics of the S_1 state. Thus, we require terms that account for both the radiative and nonradiative relaxation pathways. Initial attempts to fit single wavelength decay curves of the ^{3}ESA feature from the nsTA data to an exponential function clearly indicated the triplet decay required at least a biexponential. In fact, attempts to model the kinetics with only a monoexponential triplet decay produced results that exhibited significant intensity of the triplet feature in the singular value decomposition (SVD) of the residual data matrix, highlighting that the monoexponential decay model does not adequately describe the decay of the ^{3}ESA feature. This is consistent with other reports of multiexponential decays in the ^{3}ESA feature reflecting geminate recombination of the triplet pair on a faster timescale than un-correlated triplet decay.

In order to accommodate the biexponential decay of the ^{1}ESA, components 1 and 2 are set to equally reflect the ^{1}ESA spectrum and are weighted equally in initial intensity to reflect the weighting coefficients from the time-resolved fluorescence results (Supplementary Table S1). Components 3 and 4 are allowed to vary spectrally, but ultimately both reflect the ^{3}ESA feature. Component 1 decays into components 3 and 4 equally with a rate constant k_1, component 2 decays to the ground state with rate constant k_2, and components 3 and 4 decay to the ground state with rate constants k_3 and k_4 respectively.

Table S1. HDPP-Pent visible fs and ns TA target analysis; no parameters fixed

	k (s^{-1})	Standard Error
k_1	1.3(4) x 10^9	1.07 x 10^7
k_2	2.0(2) x 10^8	2.31 x 10^6
k_3	2.6(6) x 10^7	1.72 x 10^5
k_4	2.8(1) x 10^4	3.32 x 10^2

	t (ps)
t_1	7.4(6) x 10^2
t_2	4.9(5) x 10^3
t_3	3.7(6) x 10^4
t_4	3.5(6) x 10^7

	1	2	3	4
1				
2		k_2		
3	k_1		k_3	
4	k_1			k_4

Fitted kinetic parameters obtained from a four component model of the composite visible fs and ns TA data of HDPP-Pent: components 1 and 2 equally correspond to ^{1}ESA vectors (reflecting the biexponential decay observed from the time-resolved fluorescence measurements), components 3 and 4 similarly reflect the short- and long-lived ^{3}ESA vectors. Component 1 decays equally into components 3 and 4 with a rate k_1; components 2, 3, and 4 decay with a rate of k_2, k_3, k_4 respectively. Residual standard error 0.00175329.

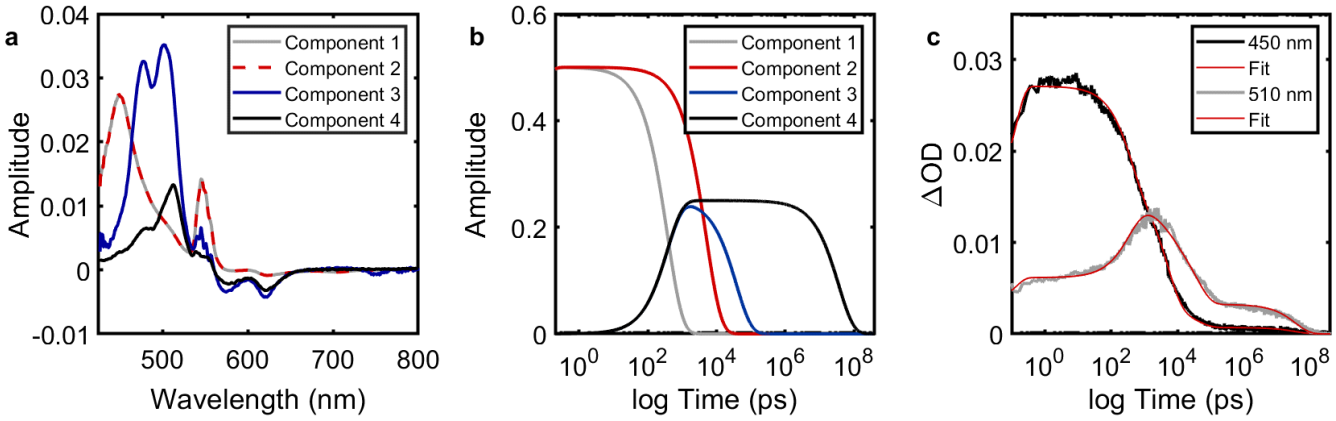

Figure S21. Glotaran target analysis (Table S1) of HDPP-Pent (50 μM, toluene) visible fs and ns TA data; no parameters fixed: (a) species associated spectra, (b) kinetic traces of fitted components, and (c) kinetic fits overlaying experimental data at 450 and 510 nm.

Table S2. HDPP-Pent visible fs and ns TA target analysis; k_1 and k_2 fixed

	k (s^{-1})	Standard Error
k_1	1.3(8) x 10^9	-
k_2	8.5(0) x 10^8	-
k_3	2.6(7) x 10^7	1.98 x 10^5
k_4	2.8(7) x 10^4	3.37 x 10^2

	t (ps)
t_1	7.2(5) x 10^2
t_2	1.1(8) x 10^4
t_3	3.7(5) x 10^4
t_4	3.4(8) x 10^7

	1	2	3	4
1				
2		k_2		
3	k_1		k_3	
4	k_1			k_4

Fitted kinetic parameters obtained from a four component model of the composite visible fs and ns TA data of HDPP-Pent: components 1 and 2 equally correspond to ^{1}ESA vectors (reflecting the biexponential decay observed from the time-resolved fluorescence measurements), components 3 and 4 similarly reflect the short- and long-lived ^{3}ESA vectors. Component 1 decays equally into components 3 and 4 with a rate k_1; components 2, 3, and 4 decay with a rate of k_2, k_3, k_4 respectively. k_1 and k_2 have been fixed given the rates from time-resolved fluorescence measurements. Residual standard error: 0.00176051.

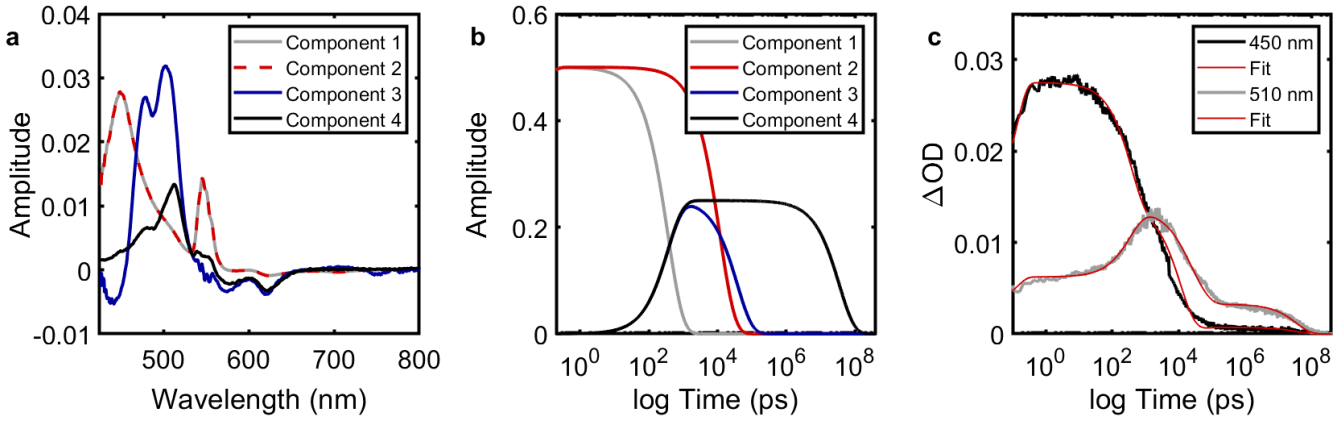

Figure S22. Glotaran target analysis (Table S2) of HDPP-Pent (50 µM, toluene) visible fs and ns TA data, k_1 and k_2 fixed: (a) species associated spectra, (b) kinetic traces of fitted components, and (c) kinetic fits overlaying experimental data at 450 and 510 nm.

Table S3. HDPP-Pent visible fsTA target analysis

	k (s^{-1})	Standard Error
k_1	2.5(6) x 10^9	3.86 x 10^7
k_2	1.7(2) x 10^8	5.20 x 10^6
k_3	1.(8) x 10^7	1.72 x 10^6
	t (ps)	
t_1	3.9(1) x 10^2	
t_2	5.8(1) x 10^3	
t_3	5.(6) x 10^4	

	1	2	3
1			
2		k_2	
3	k_1		k_3

Fitted kinetic parameters obtained from a three component model of the fsTA data of HDPP-Pent: components 1 and 2 equally correspond to ^{1}ESA vectors (reflecting the biexponential decay observed from the time-resolved fluorescence measurements), components 3 reflects the decay of the ^{3}ESA vector. Component 1 decays into component 3 with a rate k_1; components 2 and 3 decay with a rate of k_2 and k_3 respectively. Residual standard error: 0.00249052.

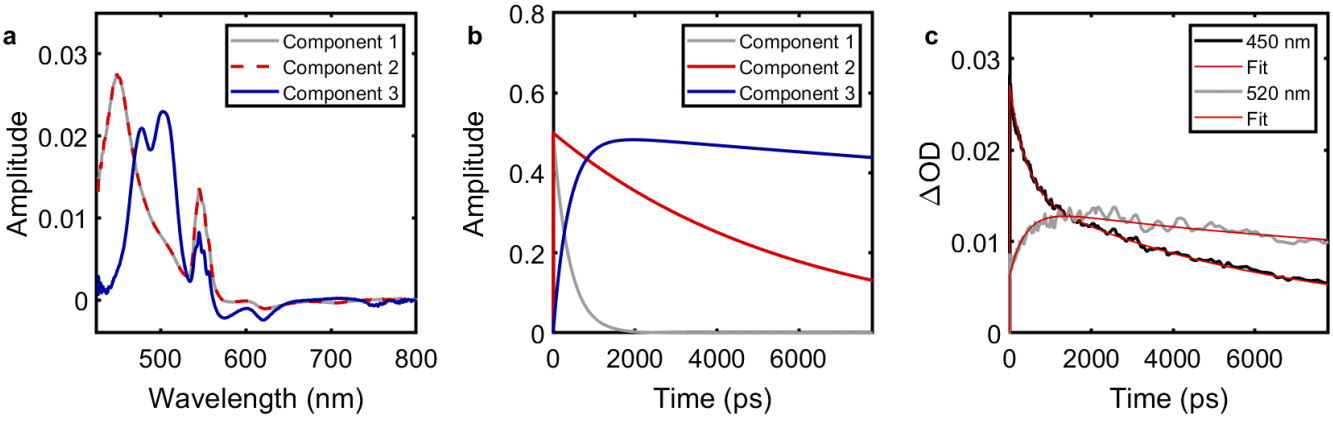

Figure S23. Glotaran target analysis (Table S3) of HDPP-Pent (50 µM, toluene) visible fsTA data: (a) species associated spectra, (b) kinetic traces of fitted components, and (c) kinetic fits overlaying experimental data at 450 and 510 nm.

Table S4. HDPP-Pent nsTA target analysis

	k (s^{-1})	Standard Error
k_1	3.5(5) x 10^7	1.76 x 10^5
k_2	2.9(4) x 10^4	2.74 x 10^2
	t (ns)	
t_1	2.8(2) x 10^1	
t_2	3.4(0) x 10^4	

	1	2
1	k_1	
2		k_2

Fitted kinetic parameters obtained from a three component model of the nsTA data of HDPP-Pent: components 1 and 2 correspond to ^{3}ESA vectors representing the biexponential decay in the feature. Components 1 and 2 decay with rate constants k_1 and k_2 respectively. Residual standard error: 0.00197139.

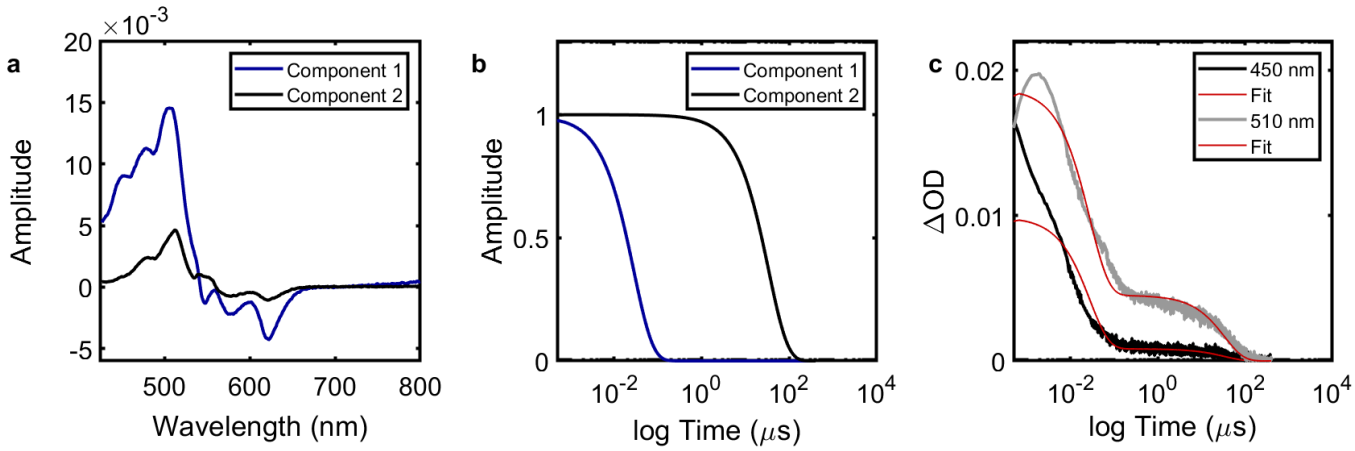

Figure S24. Glotaran target analysis (Table S4) of HDPP-Pent (50 μM, toluene) visible nsTA data: (a) species associated spectra, (b) kinetic traces of fitted components, and (c) kinetic fits overlaying experimental data at 450 and 510 nm.

$Li_2(DPP\text{-}Pent)_2$

Table S5. $Li_2(DPP\text{-}Pent)_2$ visible fs and ns TA target analysis; 3 component model

	k (s^{-1})	Standard Error
k_1	1.0(4) x 10^{10}	1.47 x 10^8
k_2	4.3(0) x 10^7	2.44 x 10^4
k_3	2.8(6) x 10^4	2.84 x 10^2

	t (ps)
t_1	96.(2)
t_2	2.3(3) x 10^4
t_3	3.5(0) x 10^7

	1	2	3
1			
2	k_1	k_2	
3	k_1		k_3

Fitted kinetic parameters obtained from a three component model of the composite fs and ns TA data of $Li_2(DPP\text{-}Pent)_2$: component 1 corresponds to a ^{1}ESA, components 2 and 3 reflect the short- and long-lived ^{3}ESA vectors. Component 1 decays equally into components 2 and 3 with a rate k_1; components 2 and 3 decay with a rate of k_2 and k_3 respectively. The final fits reported are averaged over two datasets. Residual standard error 0.00167259.

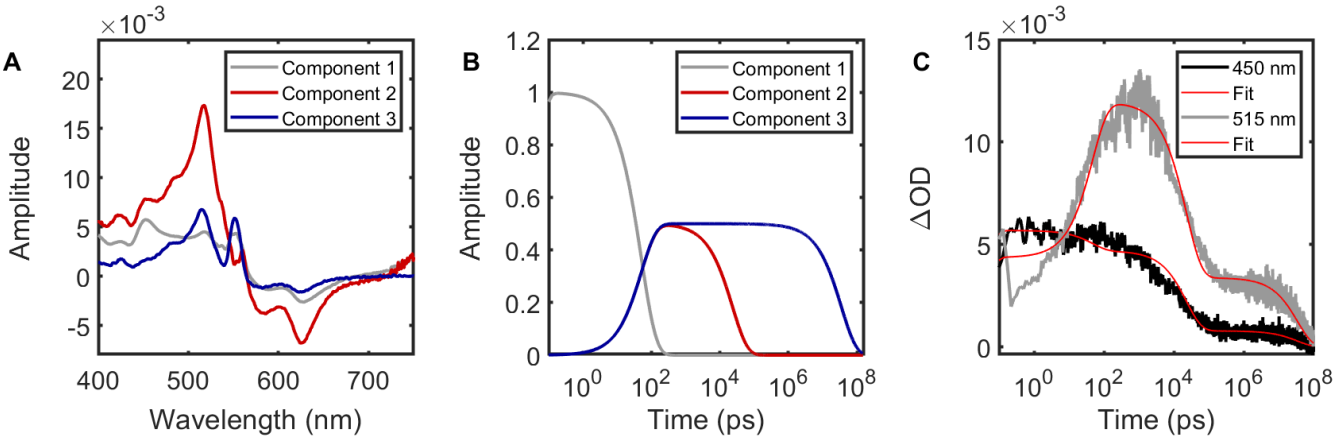

Figure S25. Glotaran target analysis (Table S5) of $Li_2(DPP\text{-}Pent)_2$ (50 µM, toluene) visible fs and ns TA data with a three component model: (a) species associated spectra, (b) kinetic traces of fitted components, and (c) kinetic fits overlaying experimental data at 450 and 515 nm. The rapid rise of the triplet feature causes a slight deviation for the fits at these early times as seen in the intensity at 515 nm in the species associated spectra of component 1.

Table S6. $Li_2(DPP\text{-}Pent)_2$ visible fs and ns TA target; 4 component model

	k (s^{-1})	Standard Error
k_1	9.0(4) x 10^9	9.66 x 10^7
k_2	9.3(9) x 10^7	2.75 x 10^5
k_3	7.(8) x 10^6	1.4 x 10^5
k_4	1.9(9) x 10^4	2.72 x 10^2

	t (ps)
t_1	1.1(1) x 10^2
t_2	1.0(7) x 10^4
t_3	1.(3) x 10^5
t_4	5.0(3) x 10^7

	1	2	3	4
1				
2	k_1	k_2		
3	k_1		k_3	
4	k_1			k_4

Fitted kinetic parameters obtained from a three component model of the composite fs and ns TA data of $Li_2(DPP\text{-}Pent)_2$: component 1 corresponds to a ^{1}ESA, components 2, 3, and 4 reflect short-, intermediate-, and long-lived ^{3}ESA vectors. Component 1 decays equally into components 2, 3, and 4 with a rate k_1; components 2, 3, and 4 decay with a rate of k_2, k_3, and k_4 respectively. The final fits reported are averaged over two datasets. Residual standard error 0.00167048.

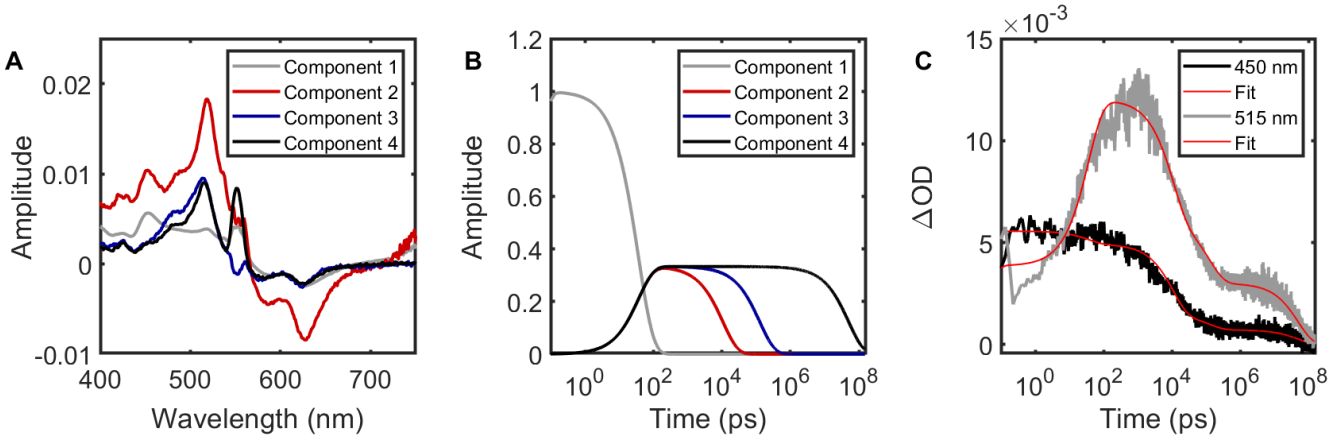

Figure S26. Glotaran target analysis (Table S5) of $Li_2(DPP\text{-}Pent)_2$ (50 µM, toluene) visible fs and ns TA data with a four component model: (a) species associated spectra, (b) kinetic traces of fitted components, and (c) kinetic fits overlaying experimental data at 450 and 515 nm. The rapid rise of the triplet feature causes a slight deviation for the fits at these early times as seen in the intensity at 515 nm in the species associated spectra of component 1.

Table S7. $Li_2(DPP\text{-}Pent)_2$ visible fsTA target analysis

	k (s^{-1})	Standard Error
k_1	1.44(0) x 10^{10}	8.786 x 10^7
k_2	2.8(6) x 10^7	3.25 x 10^5
	t (ps)	
t_1	6.94(4) x 10^1	
t_2	2.51(1) x 10^4	

	1	2
1		
2	k_1	k_2

Fitted kinetic parameters obtained from a two-component, sequential model of the fsTA data of $Li_2(DPP\text{-}Pent)_2$: component 1 corresponds to a ^{1}ESA, and component 2 reflects the ^{3}ESA vector. Residual standard error 0.00211332.

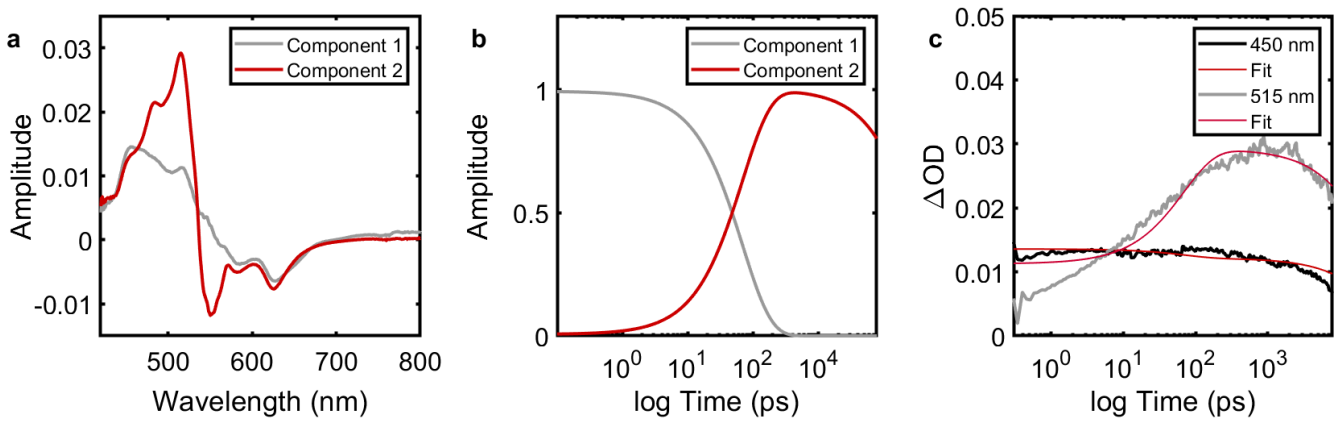

Figure S27. Glotaran target analysis (Table S6) of $Li_2(DPP\text{-}Pent)_2$ (50 µM, toluene) visible fsTA data: (a) evolution associated spectra, (b) kinetic traces of fitted components, and (c) kinetic fits overlaying experimental data at 450 and 510 nm. The rapid rise of the triplet feature causes a slight deviation for the fits at these early times as seen in the intensity at 515 nm in the species associated spectra of component 1.

Table S8. $Li_2(DPP\text{-}Pent)_2$ visible nsTA target analysis

	k (s^{-1})	Standard Error
k_1	2.60(2) x 10^7	7.978 x 10^4
k_2	2.19(1) x 10^4	9.291 x 10^1
	t (ns)	
t_1	3.84(3) x 10^1	
t_2	4.56(4) x 10^4	

	1	2
1	k_1	
2		k_2

Fitted kinetic parameters obtained from a two-component, sequential model of the nsTA data of $Li_2(DPP\text{-}Pent)_2$: components 1 and 2 correspond to the ^{3}ESA vector, reflecting a biexponential decay. Residual standard error 0.000664370.

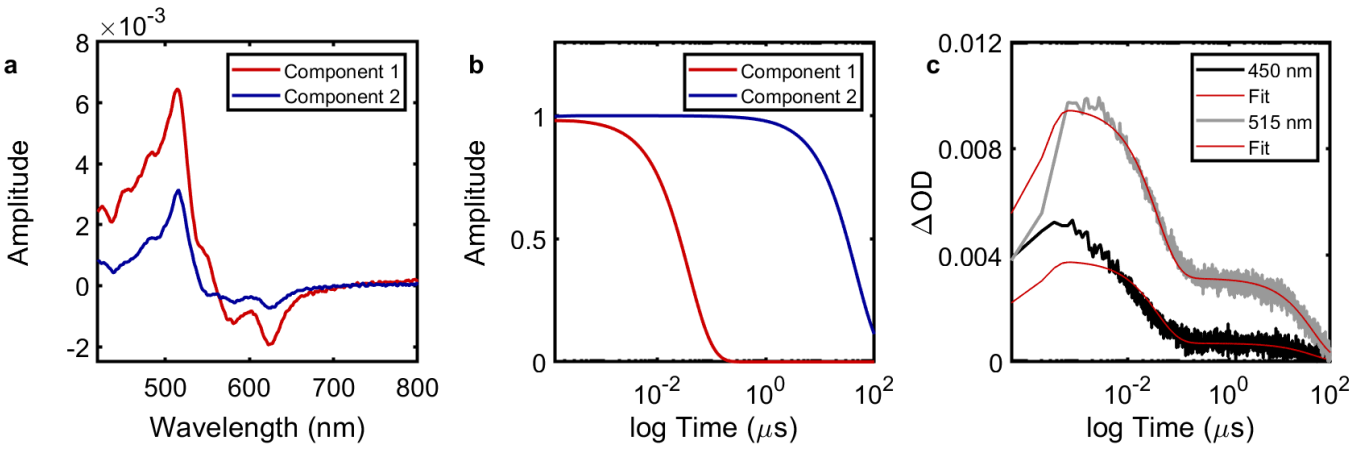

Figure S28. Glotaran target analysis (Table S7) of $Li_2(DPP\text{-}Pent)_2$ (50 μM, toluene) visible nsTA data: (a) species associated spectra, (b) kinetic traces of fitted components, and (c) kinetic fits overlaying experimental data at 450 and 510 nm.

KDPP-Pent

Table S9. KDPP-Pent visible fs and ns TA target analysis – 3 components

	k (s^{-1})	Standard Error
k_1	1.60(0) x 10^9	9.897 x 10^6
k_2	1.75(3) x 10^8	5.121 x 10^5
k_3	6.0(5) x 10^4	1.6(5) x 10^2
	t (ps)	
t_1	6.25(0) x 10^2	
t_2	5.70(5) x 10^4	
t_3	1.6(5) x 10^7	

	1	2	3
1			
2	k_1	k_2	
3	k_1		k_3

Fitted kinetic parameters obtained from a three component model of the composite fs and ns TA data of KDPP-Pent: component 1 corresponds to a ^{1}ESA, components 2 and 3 reflect the short- and long-lived ^{3}ESA vectors. Component 1 decays equally into components 2 and 3 with a rate k_1; components 2 and 3 decay with a rate of k_2 and k_3 respectively. Residual standard error 0.000864311.

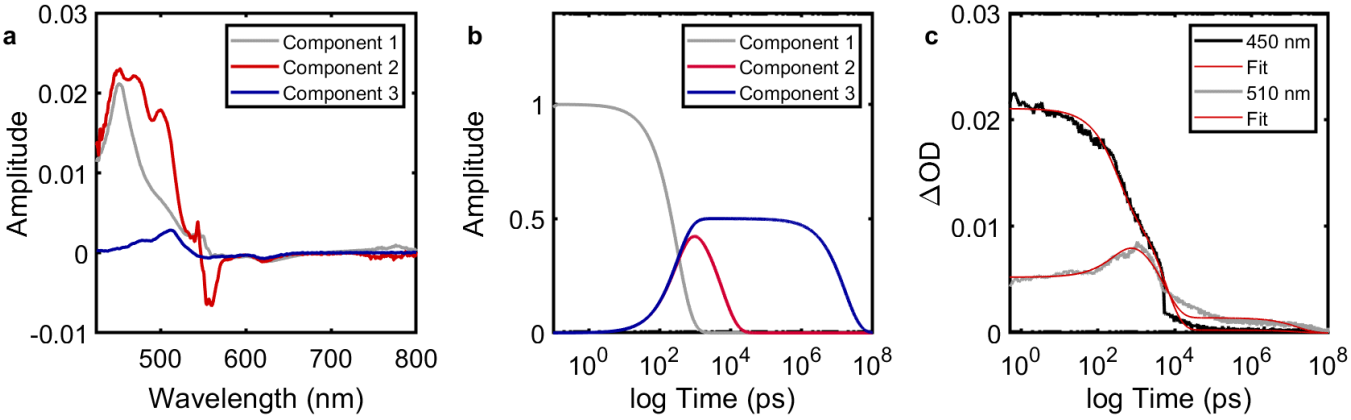

Figure S29. Glotaran target analysis (Table S8) of KDPP-Pent (50 µM, toluene) visible fs and nsTA data – 3 component fit: (a) species associated spectra, (b) kinetic traces of fitted components, and (c) kinetic fits overlaying experimental data at 450 and 510 nm.

Table S10. KDPP-Pent visible fs and ns TA target analysis – 4 components

	k (s^{-1})	Standard Error
k_1	2.2(5) x 10^9	1.71 x 10^7
k_2	2.7(5) x 10^8	2.14 x 10^6
k_3	8.7(1) x 10^7	4.85 x 10^5
k_4	3.7(2) x 10^4	4.85 x 10^2

	t (ps)
t_1	4.4(4) x 10^2
t_2	3.6(4) x 10^4
t_3	1.1(5) x 10^5
t_4	2.6(9) x 10^7

	1	2	3	4
1				
2		k_2		
3	k_1		k_3	
4	k_1			k_4

Fitted kinetic parameters obtained from a four component model of the composite fs and ns TA data of KDPP-Pent: components 1 and 2 equally correspond to ^{1}ESA vectors, components 3 and 4 similarly reflect the short- and long-lived ^{3}ESA vectors. Component 1 decays equally into components 3 and 4 with a rate k_1; components 2, 3, and 4 decay with a rate of k_2, k_3, k_4 respectively. Residual standard error 0.000862214. k_1 and k_2 have been fixed given the rates from time-resolved fluorescence measurements.

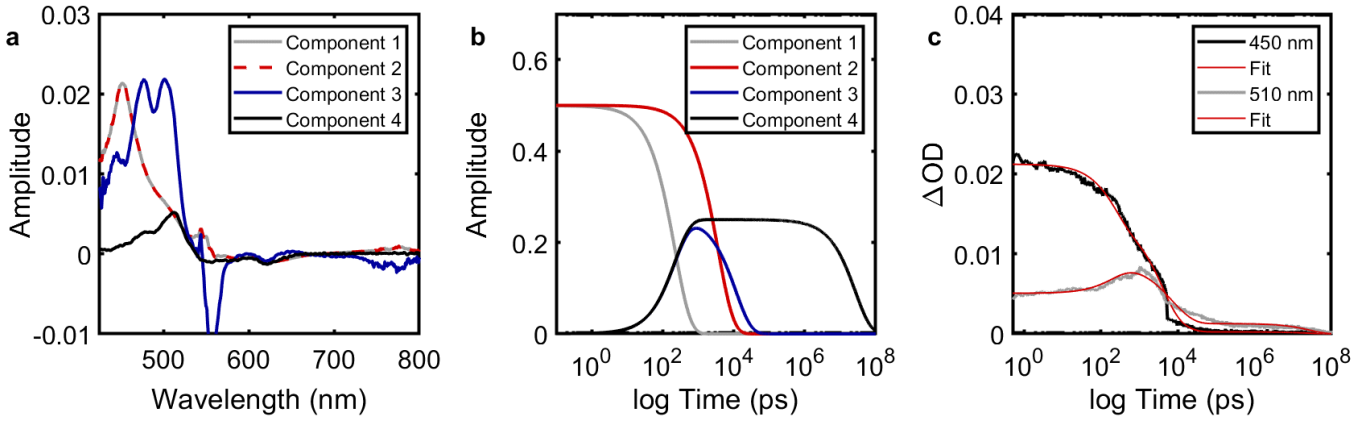

Figure S30. Glotaran target analysis (Table S9) of KDPP-Pent (50 µM, toluene) visible fs and nsTA data – four component fit: (a) species associated spectra, (b) kinetic traces of fitted components, and (c) kinetic fits overlaying experimental data at 450 and 510 nm.

Table S11. KDPP-Pent visible fsTA target analysis

	k (s^{-1})	Standard Error
k_1	2.2(7) x 10^9	2.86 x 10^7
k_2	1.4(4) x 10^8	1.14 x 10^6
	t (ps)	
t_1	4.4(1) x 10^2	
t_2	6.9(4) x 10^3	

	1	2
1		
2	k_1	k_2

Fitted kinetic parameters obtained from a two-component, sequential decay model of the fsTA data of KDPP-Pent: components 1 and 2 correspond to the ^{1}ESA and ^{3}ESA vectors, respectively. Residual standard error 0.00179745.

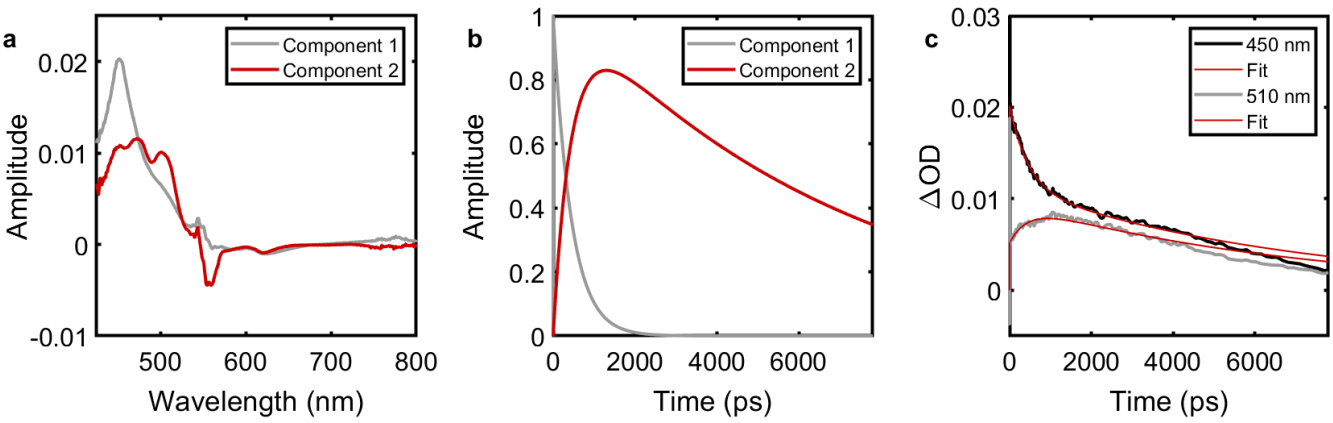

Figure S31. Glotaran target analysis (Table S10) of KDPP-Pent (50 µM, toluene) visible fsTA data: (a) evolution associated spectra, (b) kinetic traces of fitted components, and (c) kinetic fits overlaying experimental data at 450 and 510 nm.

Table S12. KDPP-Pent visible nsTA target analysis

	k (s^{-1})	Standard Error
k_1	3.1(6) x 10^7	1.27 x 10^5
k_2	2.7(3) x 10^4	1.14 x 10^2
	t (ns)	
t_1	3.1(6) x 10^1	
t_2	3.6(6) x 10^4	

	1	2
1	k_1	
2		k_2

Fitted kinetic parameters obtained from a two-component, parallel decay model of the nsTA data of KDPP-Pent: components 1 and 2 correspond to the ^{3}ESA vectors. Residual standard error 0.000674488.

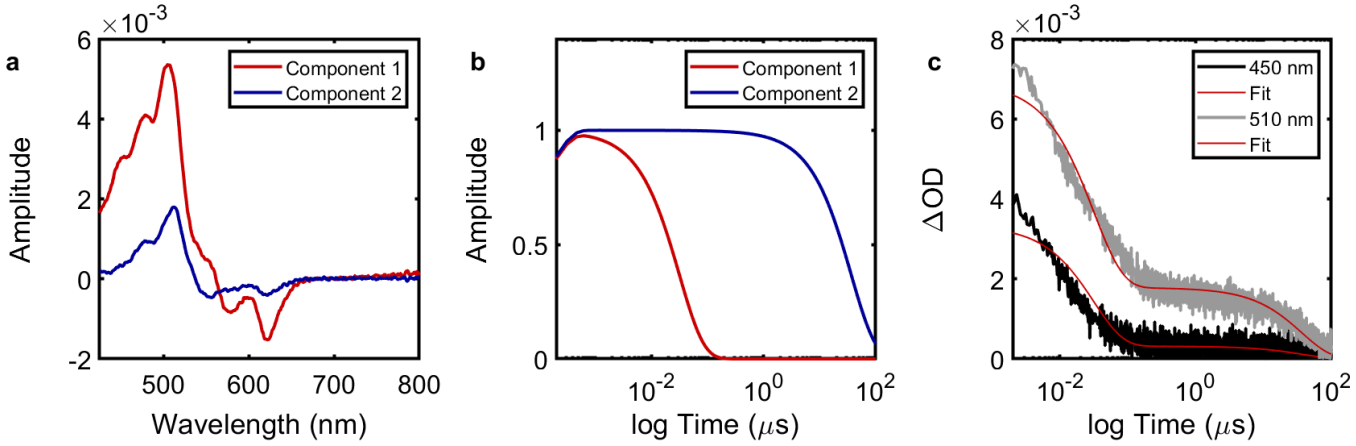

Figure S32. Glotaran target analysis (Table S11) of KDPP-Pent (50 μM, toluene) visible nsTA data: (a) evolution associated spectra, (b) kinetic traces of fitted components, and (c) kinetic fits overlaying experimental data at 450 and 510 nm.

VIII. HDPP-Pent: Triplet Extinction Coefficient Estimation

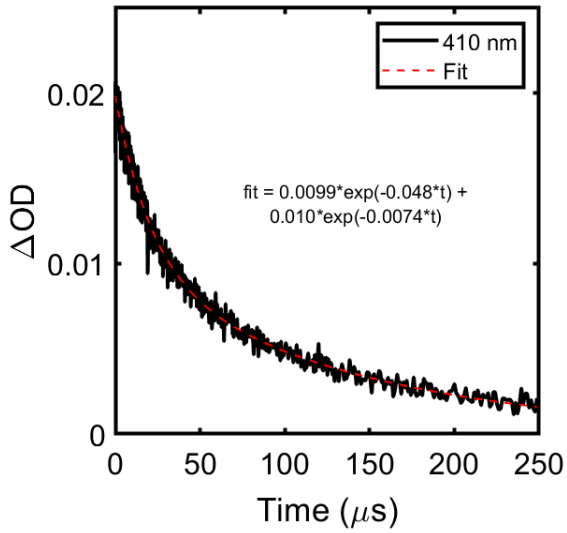

Figure S33. Anthracene (500 μM, toluene) ^{3}ESA ns transient absorption trace at 410 nm.

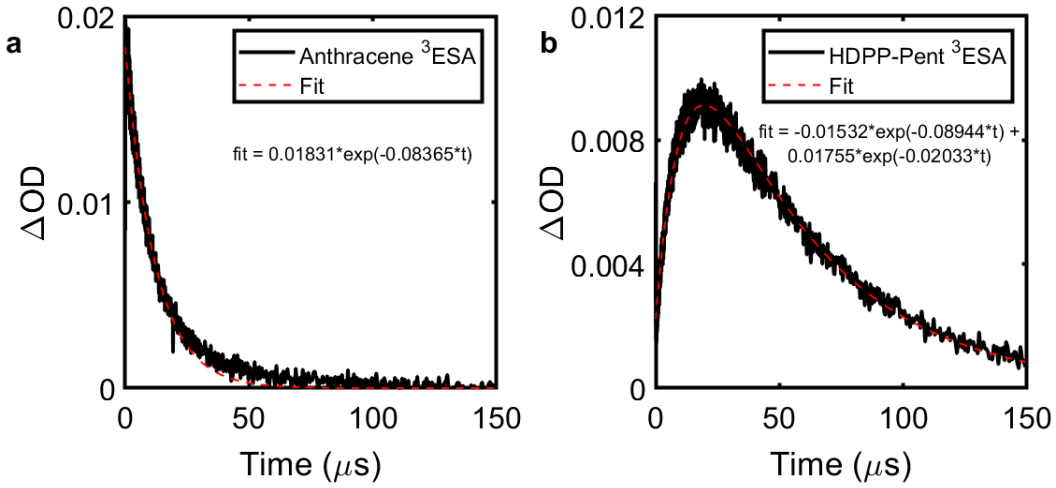

Figure S34. Photosensitization experiment (500 μM Anthracene, 10 μM HDPP-Pent in toluene): (a) Anthracene ^{3}ESA nsTA kinetic trace at 410 nm, (b) HDPP-Pent ^{3}ESA nsTA kinetic trace at 510 nm.

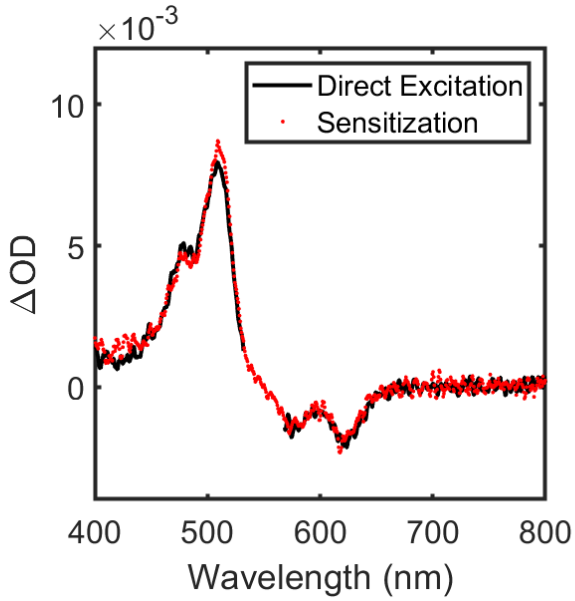

Figure S35. Comparison between the transient absorption spectrum of HDPP-Pent at long delay times (50 ns) after direct photosensitization with 550 nm light and the transient absorption spectrum of the photosensitized anthracene (500 μM) and HDPP-Pent (10 μM) after exciting anthracene at 360 nm at delay times (35 μs) past the decay of the anthracene triplet ESA. In the photosensitization experiment, we expect the anthracene triplet to be transferred to HDPP-Pent, resulting in the observation of the triplet transient absorption spectrum of HDPP-Pent at long delay times. This same spectrum is observed in the direct excitation experiment at long delay times, indicating that these spectral features are indeed associated with the HDPP-Pent T_1 state. The residual pump scatter at 550 nm was excised from the direct excitation spectrum.

The Anthracene (500 μM) and HDPP-Pent (10 μM) photosensitization experiment will be used to demonstrate the calculation of the HDPP-Pent ^{3}ESA extinction coefficient given the reported Anthracene ^{3}ESA molar absorptivity (42,000 M^{-1} cm^{-1}).[4–7] This is accomplished by setting the concentrations of Anthracene and HDPP-Pent triplets to be equal in the Beer-Lambert regime and solving for ^{3}HDPP-Pent ε as in Equation 2:

$$c_{^3Anth} = c_{^3HDPP-Pent}$$

$$\frac{\Delta OD_{^3Anth}}{\varepsilon_{^3Anth} \cdot l} = \frac{\Delta OD_{^3HDPP-Pent}}{\varepsilon_{^3HDPP-Pent} \cdot l}$$

$$\varepsilon_{^3HDPP-Pent} = \frac{\Delta OD_{^3HDPP-Pent}}{\Delta OD_{^3Anth}} \cdot \varepsilon_{^3Anth} \qquad Eq\ (2)$$

The assumption underlying this equation is that the energy transfer efficiency is near unity – that the concentration of anthracene triplets fully transfers into HDPP-Pent triplets. In order to fulfill this estimation, corrections must be made to the ^{3} HDPP-Pent ΔOD to account for triplet transfer efficiency (Φ_{ET}) and the relative rate of the rise and decay of the HDPP-Pent ^{3}ESA ($\Phi_{T(decay)}$).

$$\Phi_{ET} = \frac{k_{sens}}{k_{sens} + k_{intrinsic}}$$

$$\Phi_{ET} = \frac{0.08365}{0.08365 + 0.048} = 0.64$$

$$\Phi_{T(decay)} = \frac{k_{T(rise)}}{k_{T(rise)} + k_{T(decay)}}$$

$$\Phi_{T(decay)} = \frac{0.08944}{0.08944 + 0.02033} = 0.81$$

The corrected ^{3}HDPP-Pent ΔOD (ΔOD_{corr}) can thus be estimated and the HDPP-Pent ^{3}ESA extinction coefficient can be calculated as in Equation 2:

$$\Delta OD_{corr} = \frac{\Delta OD\ {}^3{}_{HDPP-Pent}}{\Phi_{ET} \cdot \Phi_{T(decay)}} = \frac{0.0091}{0.64 \cdot 0.81}$$

$$\Delta OD_{corr} = 0.0176$$

$$\varepsilon\ {}^3{}_{HDPP-Pent} = \frac{0.0176}{0.0183} \cdot (42{,}000\ M^{-1}cm^{-1})$$

$$\varepsilon\ {}^3{}_{HDPP-Pent} = 40{,}393\ M^{-1}cm^{-1}$$

This process is repeated for each concentration of HDPP-Pent (10, 20, 50, 100 μM) and the results are compiled in Figure S35. As can be seen, the calculated ^{3}HDPP-Pent extinction coefficient approaches a limit of ~ 49,000 M^{-1} cm^{-1} as the concentration of HDPP-Pent is increased (i.e. the triplet energy transfer efficiency approaches unity).

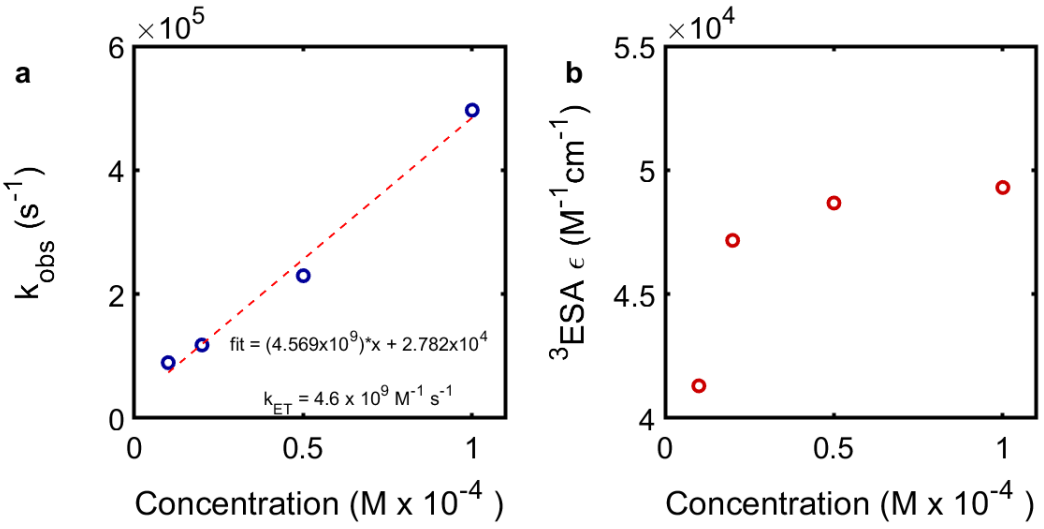

Figure S36. Concentration-dependent photosensitization experiments between Anthracene (500 μM) and HDPP-Pent (X μM, X = 10, 20, 50, 100): (a) observed energy transfer rate (k_{obs}) vs HDPP-Pent concentration, fitted to a linear function, the slope of which gives the bimolecular rate constant (k_{ET}); (b) calculated HDPP-Pent ^{3}ESA extinction coefficient vs HDPP-Pent concentration.

IX. HDPP-Pent: Triplet Yield Estimation

In order to estimate the triplet yield, we can use Equation 3. As a note, we refer to $[T_1]$ as the concentration of excited triplet states without differentiation between triplet pair (T_1T_1) and free triplet (T_1) states.

$$Triplet\ \%\ Yield = \frac{[T_1]}{[S_1]} \cdot 100 \qquad Eq\ (3)$$

i. Concentration of Excited Singlets

Let us first consider the maximum concentration of excited singlets generated. This has been previously estimated using the ground state bleach (GSB) feature. However, it must be noted in the case of HDPP-Pent that the shape and intensity of the GSB changes over the course of the transient absorption experiment in a way that suggests there is a complex overlap of GSB and ESA features in the spectrum. This makes the GSB unreliable in the evaluation of the triplet yield. The concentration of excited singlets may alternatively be estimated as the product of the number of photons per pulse and the ratio of pump intensity before and after the sample (I/I_0) divided by the product of Avogadro's number (N_A) and the excitation volume (V):[8]

$$[\boldsymbol{S_1}] = \frac{\left(\frac{\boldsymbol{photons}}{\boldsymbol{pulse}}\right) \cdot \left(\frac{\boldsymbol{I}}{\boldsymbol{I_0}}\right)}{\boldsymbol{N_A \cdot V}}$$

$$\left(\frac{photons}{pulse}\right) = \frac{power}{(rep\ rate) \cdot \left(\frac{energy}{photon}\right)}$$

$$\left(\frac{I}{I_0}\right) = 1 - 10^{-A}$$

$$V = \pi r^2 l$$

Each component may be first evaluated individually. The photons per pulse can be derived from the excitation power (100 μW), the laser repetition rate (1000 s^{-1}), and the energy per photon (as calculated by the product of Planck's constant h and the frequency of 550 nm light). I/I_0 can be calculated as the difference from unity of ten raised to the negative power of the sample absorbance at 550 nm (0.11). The excitation volume is assumed to be cylindrical using the radius of the excitation spot (0.013 cm) and the path length of the sample (0.2 cm).

$$\left(\frac{photons}{pulse}\right) = \frac{1 \times 10^{-4}\, W}{(1{,}000\, s^{-1}) \cdot (3.61 \times 10^{-19}\, J)} = 2.77 \times 10^{11}\, pulse^{-1}$$

$$\left(\frac{I}{I_0}\right) = 1 - 10^{-0.11} = 0.2238$$

$$V = \pi \cdot (1.30 \times 10^{-2}\, cm)^{2} \cdot (0.2\, cm) \cdot (0.001\, L\, cm^{-3}) = 1.06 \times 10^{-7}\, L$$

$$[S_1] = \frac{(2.77 \times 10^{11}) \cdot (0.2238)}{(6.022 \times 10^{23}) \cdot (1.06 \times 10^{-7})} = 9.7 \times 10^{-7}\, M$$

ii. Concentration of Excited Triplets

The concentration of HDPP-Pent triplets may be estimated from the extinction coefficient of the ^{3}ESA at 510 nm as derived above and the maximum ΔOD value at 510 nm from the experimental transient absorption data. However, from the time-resolved luminescence data and the target fitting, it is apparent that when the TA ^{3}ESA at 510 nm reaches its maximum intensity (t ~ 1.4 ns), there is contribution to this intensity from the ^{1}ESA. The fit may be used to decompose the ΔOD at 510 nm to its contributions from the ^{1}ESA and ^{3}ESA, and the triplet contribution may be used to estimate the corrected triplet yield.

The target fitting as shown in Figure S21 gives a maximum ΔOD_{510nm} of 0.0128. The contributions of the different component vectors to the target fit can be decomposed from the kinetic traces (Figure S21b), which provides a weighting coefficient or effective concentration for each vector at 1.4 ns. The SAS (Figure S21a) provide the relative molar extinction of each vector at 510 nm. Taking the weighted sum of the first and second vectors gives the ΔOD contribution of the ^{1}ESA at 510 nm. Likewise, taking the weighted sum of the third and fourth vectors gives the relative ΔOD contribution of the ^{3}ESA. These values are collected in Table S12.

Table S13. Estimation of ^{1}ESA and ^{3}ESA ΔOD contributions at 510 nm in the transient absorption spectrum of HDPP-Pent (50 μM, toluene).

component	1	2	3	4
Relative contribution at 1.4 ns	0.0103	0.4437	0.2379	0.2448
Intensity of SAS at 510 nm	0.0062	0.0062	0.0285	0.0180
	^{1}ESA		^{3}ESA	
?OD_{510nm} contribution at 1.4 ns	0.0028		0.010	

The maximum concentration of triplets can then be estimated in the Beer-Lambert regime and the triplet yield can be thus calculated.

$$[T_1] = \frac{\Delta OD_{510nm}}{\varepsilon\,{}^{3}{}_{DPP-Pent} \cdot l}$$

$$[T_1] = \frac{0.010}{(49{,}000) \cdot (0.2)} = 1.0 \times 10^{-6}\,M$$

$$Triplet\ Yield = \frac{[T_1]}{[S_1]} \cdot 100 = \frac{1.0 \times 10^{-6}\,M}{9.7 \times 10^{-7}\,M} \cdot 100$$

$$Triplet\ Yield \sim 100\ \%$$

X. $Li_2(DPP\text{-}Pent)_2$: Triplet Extinction Coefficient Estimation

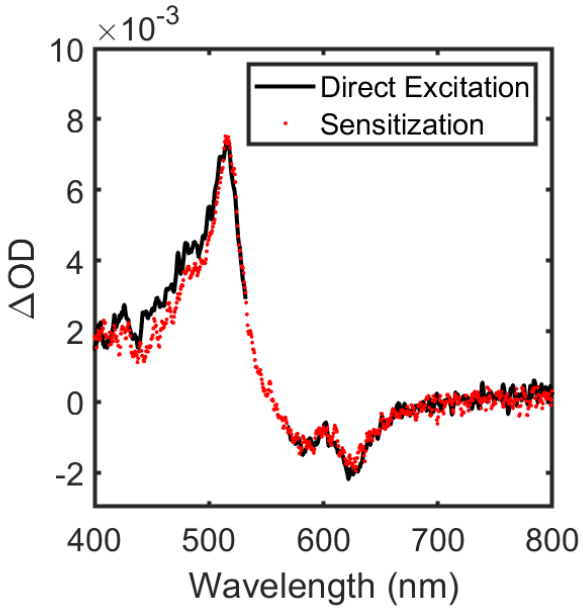

Figure S37. Comparison between the transient absorption spectrum of $Li_2(DPP\text{-}Pent)_2$ at long delay times (20 ns) after direct photosensitization with 550 nm light and the transient absorption spectrum of the photosensitized anthracene (500 μM) and $Li_2(DPP\text{-}Pent)_2$ (50 μM) after exciting anthracene at 360 nm at delay times (100 μs) past the decay of the anthracene triplet ESA. In the photosensitization experiment, we expect the anthracene triplet to be transferred to $Li_2(DPP\text{-}Pent)_2$, resulting in the observation of the triplet transient absorption spectrum of $Li_2(DPP\text{-}Pent)_2$ at long delay times. This same spectrum is observed in the direct excitation experiment at long delay times, indicating that these spectral features are indeed associated with the $Li_2(DPP\text{-}Pent)_2$ T_1 state. The residual pump scatter at 550 nm was excised from the direct excitation spectrum.

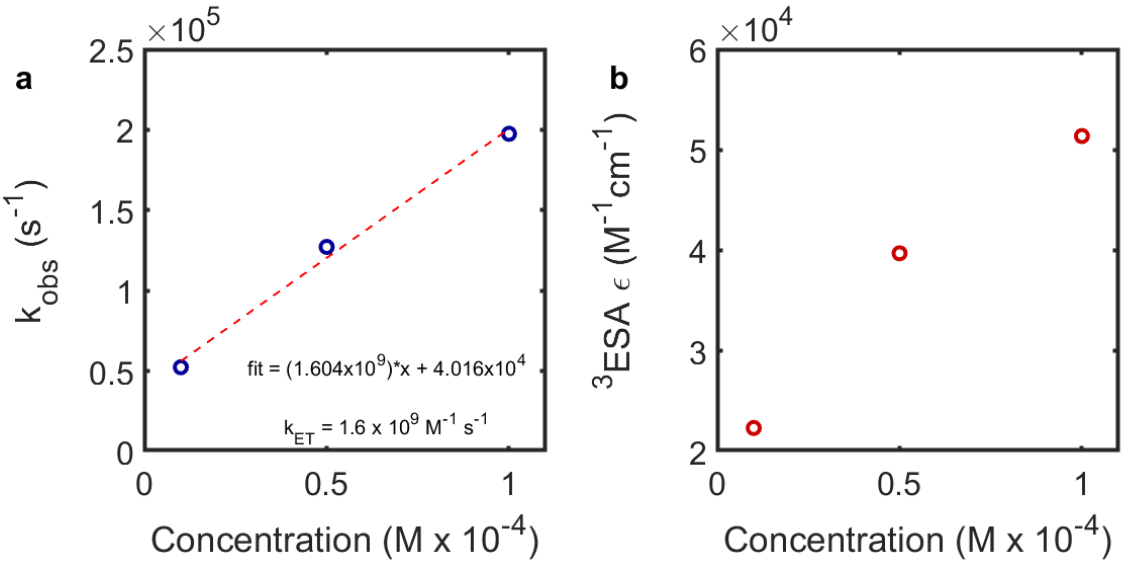

Figure S38. Concentration-dependent photosensitization experiments between Anthracene (500 μM) and Li_2(DPP-Pent)$_2$ (X μM, X = 10, 50, 100): (a) observed energy transfer rate (k_{obs}) vs Li_2(DPP-Pent)$_2$ concentration (based on formula weight), fitted to a linear function, the slope of which gives the bimolecular rate constant (k_{ET}); (b) calculated Li_2(DPP-Pent)$_2$ ^{3}ESA extinction coefficient vs Li_2(DPP-Pent)$_2$ concentration.

XI. $Li_2(DPP\text{-}Pent)_2$: Triplet Yield Estimation

i. Method: extinction coefficient

As with HDPP-Pent, the concentration of excited singlets is first estimated using the energy of the 550 nm pump excitation, the absorbance of the sample at 550 nm (0.0711), and the excitation volume (1.06×10^{-7} L).

$$[S_1] = \frac{(2.77 \times 10^{11}) \cdot (0.1489)}{(6.022 \times 10^{23}) \cdot (1.06 \times 10^{-7})} = 6.5 \times 10^{-7}\ M$$

As we do not have evidence to suggest there is significant singlet population overlapped with the triplet ESA at its maximum in the TA data of $Li_2(DPP\text{-}Pent)_2$, we directly estimate the triplet yield without correction from the fitted data.

$$[T_1] = \frac{\Delta OD_{510nm}}{\varepsilon\ {}^3{}_{LiDPP-Pent} \cdot l}$$

$$[T_1] = \frac{0.013}{(52{,}000) \cdot (0.2)} = 1.27 \times 10^{-6}\ M$$

$$Triplet\ Yield = \frac{[T_1]}{[S_1]} \cdot 100 = \frac{1.27 \times 10^{-6}\ M}{9.7 \times 10^{-7}\ M} \cdot 100$$

$$Triplet\ Yield \sim 195\ \%$$

ii. Method: ground state bleach

We can estimate the triplet yield in Li_2(DPP-Pent)$_2$ via the ground state bleach in the method of Eaton et al.[9] The percentage of excited molecules estimated from the energy density of the 550 nm pump is approximately 1.1%, and using the ground state absorbance at 625 nm (0.2), we can estimate the expected ground state bleach intensity of -0.0022. From this we can estimate a triplet yield of ~ 186%.

$$Predicted\ Max\ \Delta OD_{625\,nm} = -2.2\ mOD$$

$$Experimental\ Max\ \Delta OD_{625\,nm} = -4.1\ mOD$$

$$Triplet\ Yield = \frac{-4.1}{-2.2} \cdot 100 \sim 186\ \%$$

XII. Comparison Between Singlet Fission Rates and Triplet Lifetimes

Table S14. Comparison between singlet fission (τ_{SF}) and triplet lifetimes (τ_T) for HDPP-Pent, Li_2(DPP-Pent)$_2$, KDPP-Pent, and previously reported bipentacene systems *ortho*-**2**, *meta*-**2**, and *para*-**2** (in benzonitrile),[10] BP0, BP1, BP2,[11] TFM, BCO, Spi, and EBD (in chloroform),[12] PD, and PT.[13] The compounds are referenced using the moniker given in their respective texts, and structures are provided for each following the table. Here, τ_T is used generally for the fitted lifetimes of the triplet features in the transient absorption spectrum, encompassing both ^{M}(TT) – the shorter lifetime(s) – and uncorrelated triplet lifetimes where applicable. A comprehensive review of lifetimes in covalently linked dimers appears in Korovina et al.[14]

	τ_{SF}	τ_T
ortho-**2**	500 fs	12 ps
meta-**2**	63 ps	2.2 ns
para-**2**	2.7 ps	17.3 ps
BP0	760 fs	450 ps
BP1	20 ps	16.5 ns
BP2	220 ps	270 ns (1)
TFM	49.7 ps	531 ns (1), 23.0 μs (2)
BCO	20 ns	1.8 μs (1), 18.0 μs (2)
Spi	54.5 ps	705 ns (1), 19.6 μs (2)
EBD	10.4 ps	174 ns (1), 24.3 μs (2)
PD	435 ps	8.3 ns (1); 87 ns (2); 25 μs (3)
PT	147 ps	12 ns (1); 70 ns (2); 32 μs (3)
HDPP-Pent	730 ps	38 ns (1); 36 μs (2)
Li_2(DPP-Pent)$_2$	100 ps	23 ns (1); 35 μs (2)
KDPP-Pent	400 – 600 ps	12 ns (1); 27 μs (2)

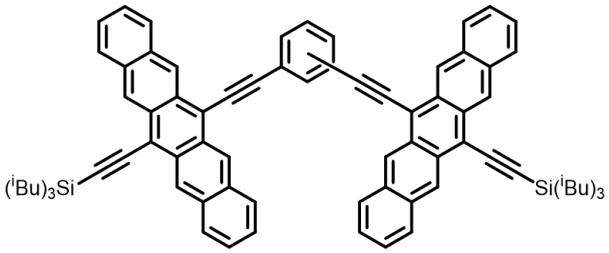

*ortho-, meta-, and para-***1**

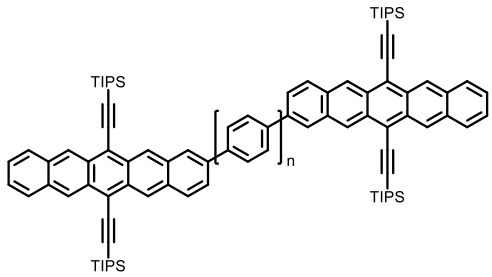

BPn (n=0,1,2)

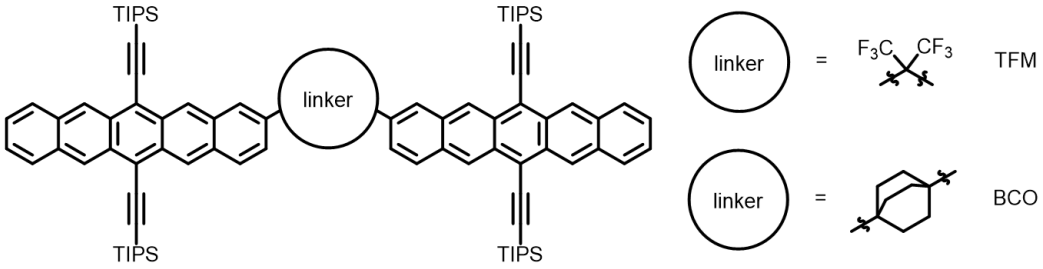

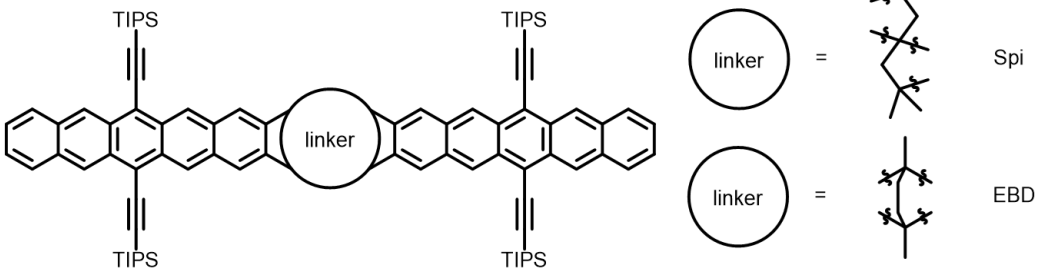

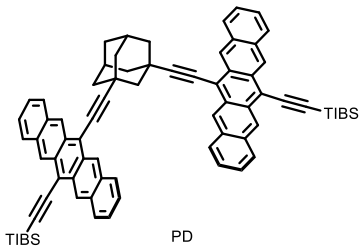

PD

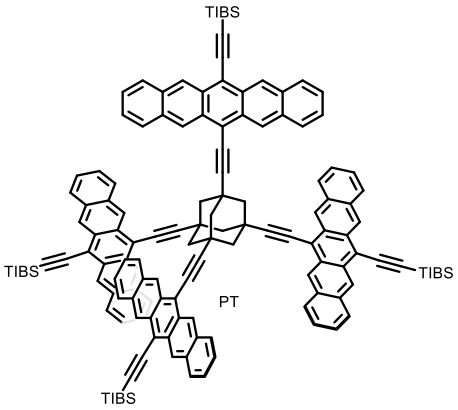

PT

XIII. ^{1}H and ^{13}C NMR

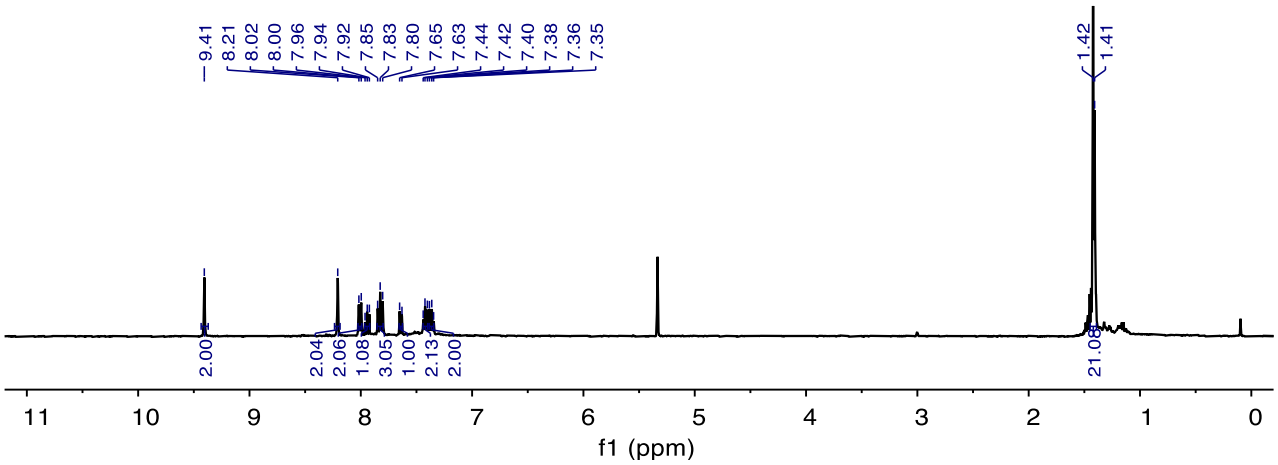

Figure S39. ^{1}H NMR spectrum of PentPyBr (400 MHz, $CDCl_3$).

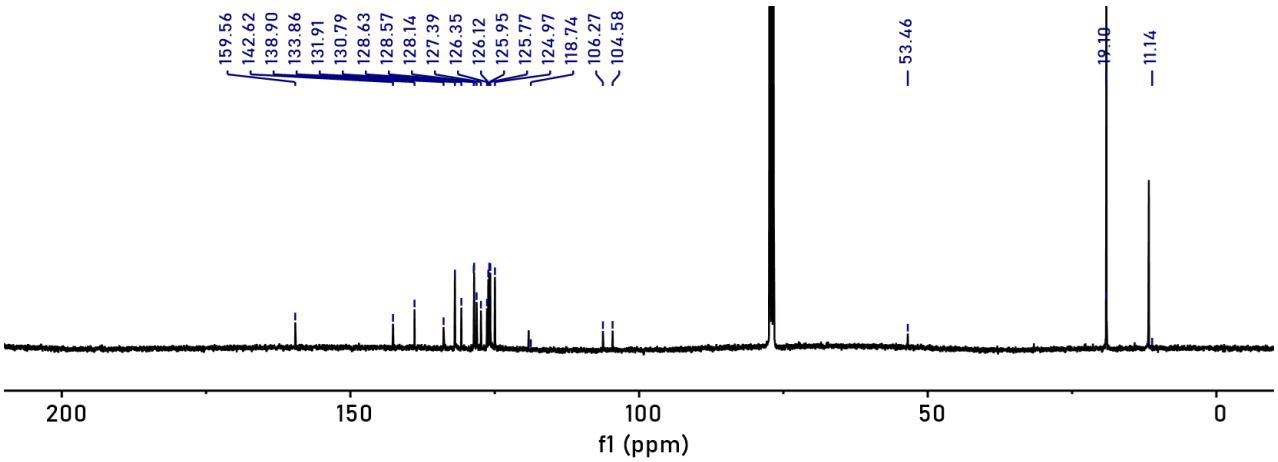

Figure S40. ^{13}C NMR spectrum of PentPyBr (400 MHz, $CDCl_3$).

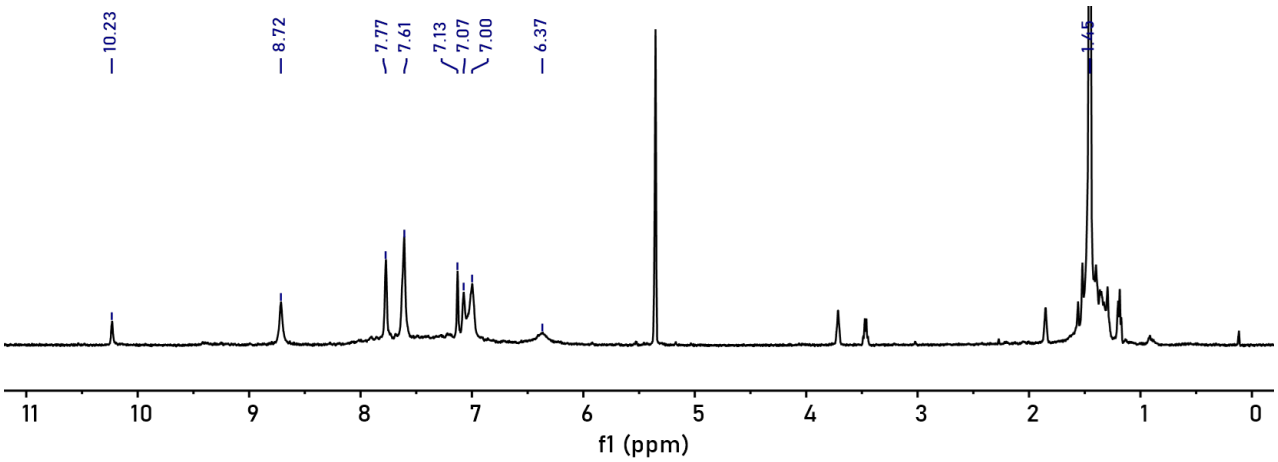

Figure S41. ^{1}H NMR spectrum of HDPP-Pent (400 MHz, CD_2Cl_2).

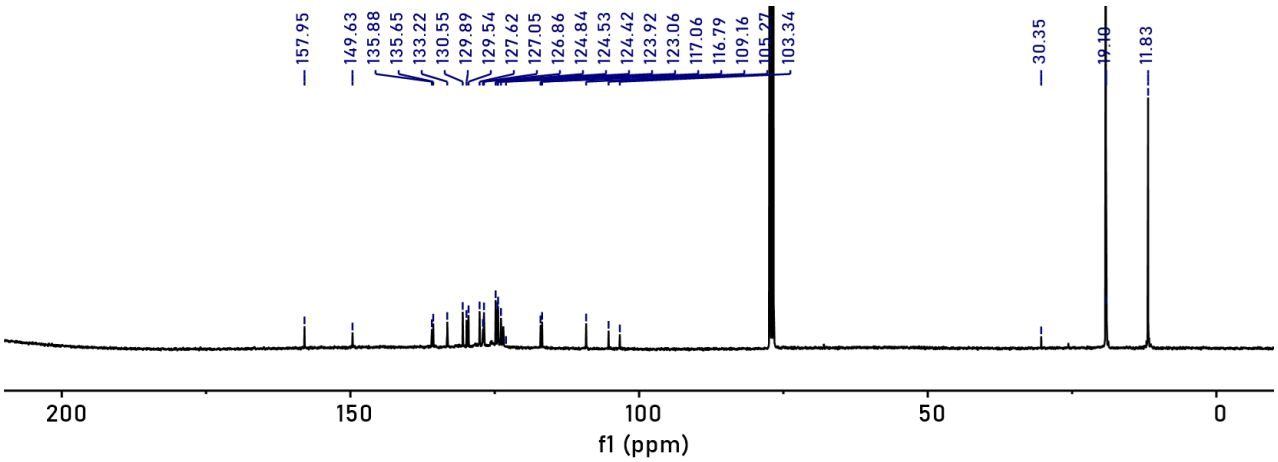

Figure S42. ^{13}C NMR spectrum of HDPP-Pent (400 MHz, $CDCl_3$).

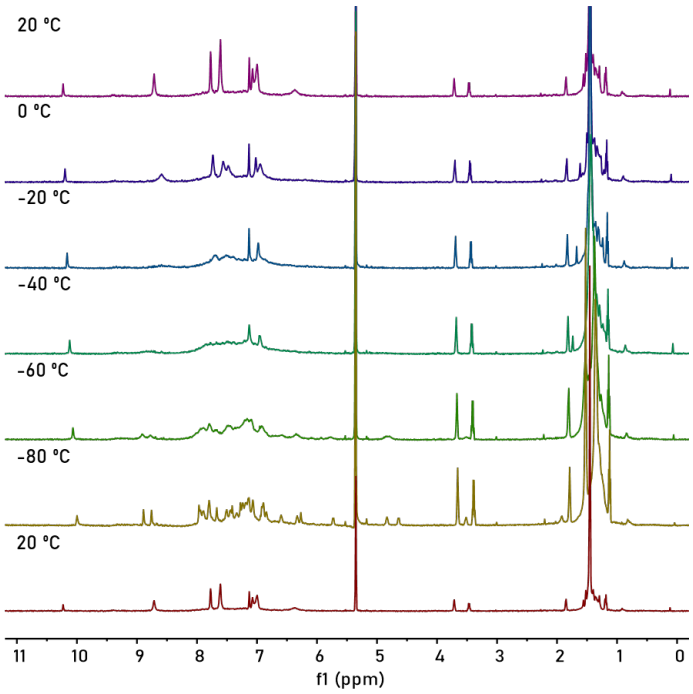

Figure S43. Variable temperature ^{1}H NMR spectra of HDPP-Pent (400 MHz, CD_2Cl_2).

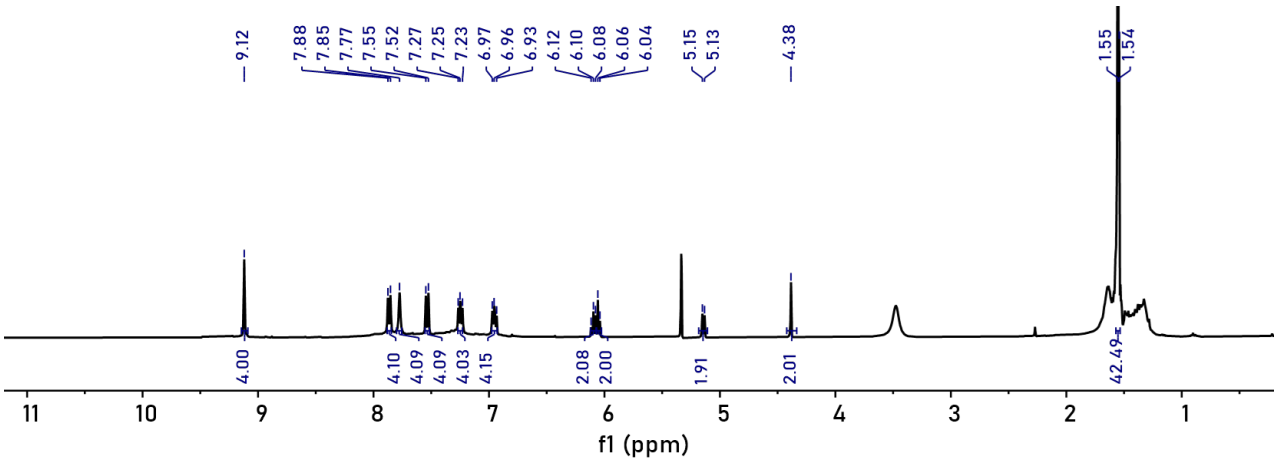

Figure S44. ^{1}H NMR spectrum of $Li_2(DPP\text{-}Pent)_2$ (400 MHz, CD_2Cl_2).

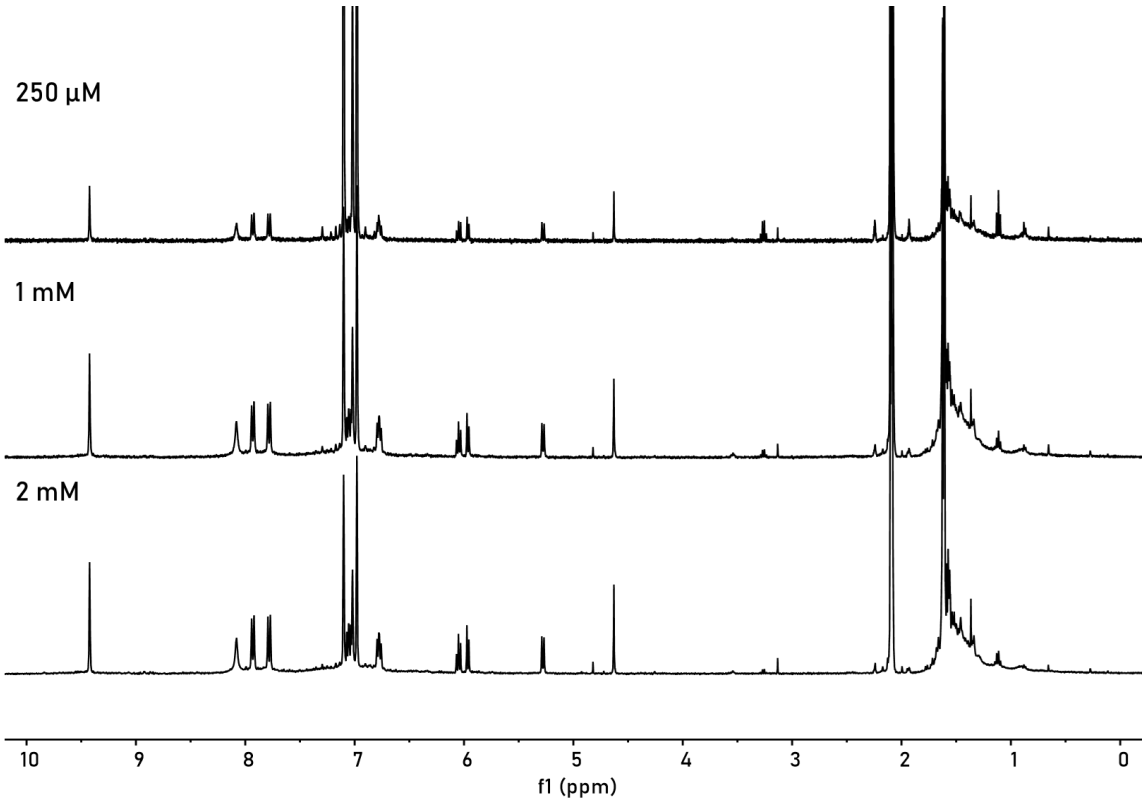

Figure S45. ^{1}H NMR spectrum of $Li_2(DPP\text{-}Pent)_2$ at different concentrations in toluene-d8 (400 MHz, toluene-d8).

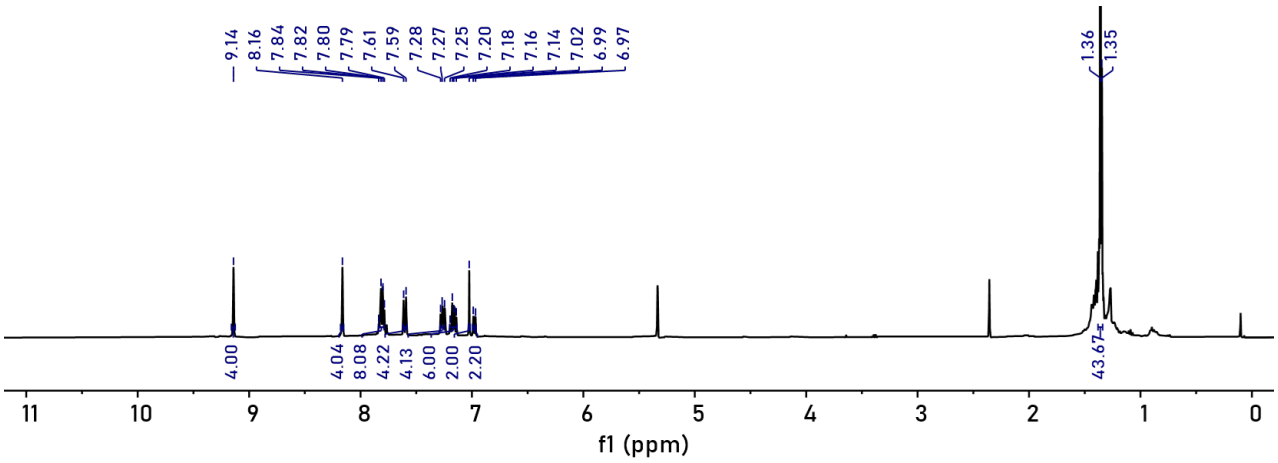

Figure S46. ^{1}H NMR spectrum of KDPP-Pent (400 MHz, CD_2Cl_2).

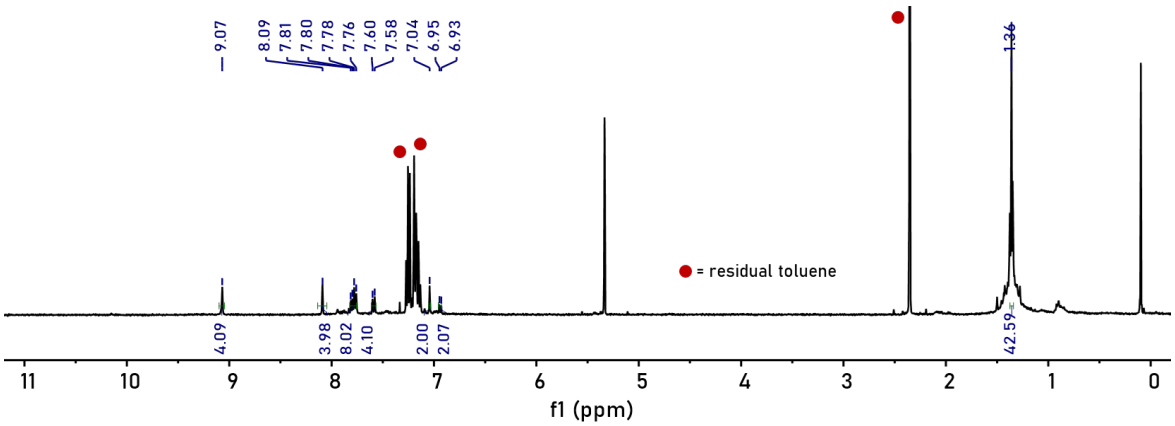

Figure S47. ^{1}H NMR spectrum of NaDPP-Pent (400 MHz, CD_2Cl_2). A significant amount of toluene (peaks at 2.34, 7.14, 7.24 ppm) remained in the sample post-synthesis despite extensive drying *in vacuo*. Further handling and attempts to fully remove the toluene led to a small degree of decomposition. The toluene multiplets in the aromatic region mask three peaks expected in the compound but can be inferred from cross peaks detected in the COSY and ROESY experiments.

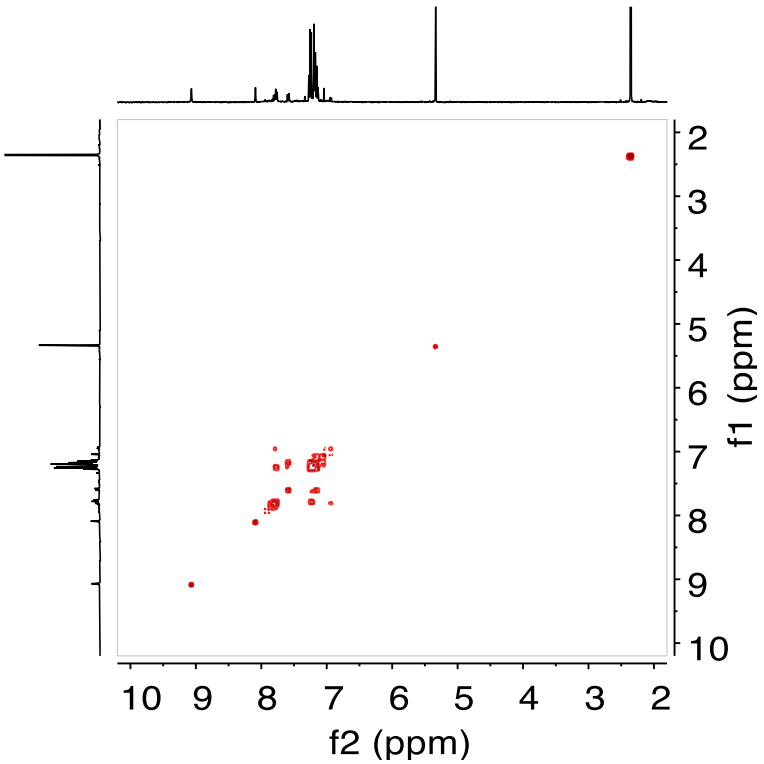

Figure S48. Gradient COSY spectrum of NaDPP-Pent (400 MHz, CD_2Cl_2).

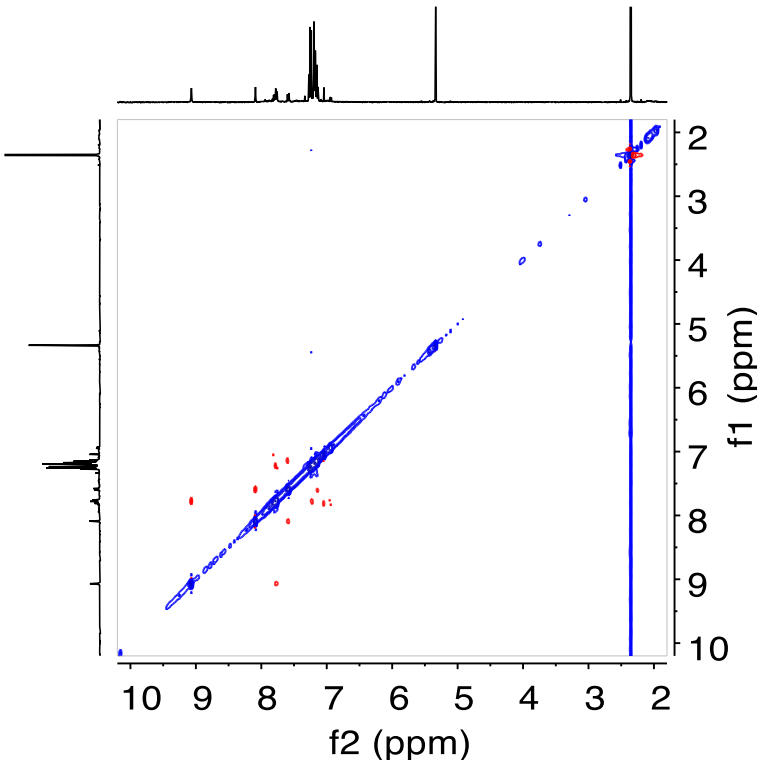

Figure S49. 2D ROESY spectrum of NaDPP-Pent (400 MHz, CD_2Cl_2).

XIV. $Li_2(DPP\text{-}Anth)_2$ Crystallographic Information

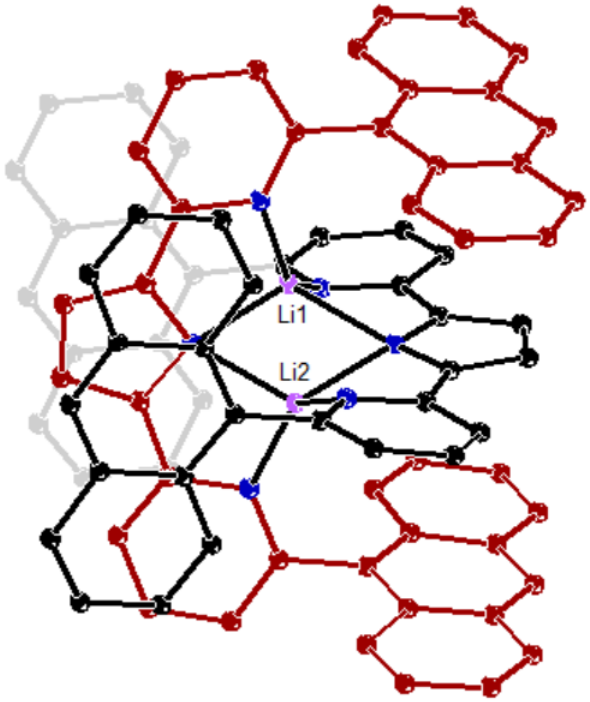

Figure S50. X-ray crystal structure of $Li_2(DPP\text{-}Anth)_2$. The DPP-Anth ligand 1 and 2 are coded as black and red, respectively. Ellipsoids are drawn at the 50% probability level.

Table S14. Crystal and refinement data for $Li_2(DPP\text{-}Anth)_2$

	$Li_2(DPP\text{-}Anth)_2$
CCDC	2031858
Empirical formula	$C_{84}H_{52}Li_2N_6$
Formula weight	1158.46
Temperature/K	100
Crystal System	Triclinic
Space group	P -1
a/Å	14.6365(8)
b/Å	15.1790(7)
c/Å	16.9748(11)
α/°	69.030(4)
β/°	68.970(5)
γ/°	70.059(4)
Volume/$Å^3$	3187.6
Z	2
$\rho_{calc}g/cm^3$	1.296
μ/mm^{-1}	1.331
F(000)	1297.0
Radiation	Cu Kα (λ = 1.54178)
2θ range for data collection	5.8 to 158.22
Index ranges	$-16 \leq h \leq 18$, $-18 \leq k \leq 14$, $-8 \leq l \leq 20$
Reflection collected	9802
Independent reflections	7982 [R_{int} = 0.0820, R_{sigma} = 0.1123]
Data/restraints/parameters	7982/0/856
Goodness-of-fit on F^2	1.081
Final R indexes [I>=2σ (I)]	R_1 = 0.0991, wR_2 = 0.2473
Final R indexes [all data]	R_1 = 0.1716, wR_2 = 0.2991
Largest diff. peak/hole/e $Å^{-3}$	1.16/-1.09

1. Lehnherr, D., McDonald, R. & Tykwinski, R. R. Exploring Electronically Polarized Pentacenes. *Org. Lett.* **10**, 4163–4166 (2008).
2. Seechurn, C. C. C. J., Sivakumar, V., Satoskar, D. & Colacot, T. J. Iridium-Catalyzed C–H Borylation of Heterocycles Using an Overlooked 1,10-Phenanthroline Ligand: Reinventing the Catalytic Activity by Understanding the Solvent-Assisted Neutral to Cationic Switch. *Organometallics* **33**, 3514–3522 (2014).
3. Snellenburg, J. J., Laptenok, S., Seger, R., Mullen, K. M. & Stokkum, I. H. M. van. Glotaran: A Java-Based Graphical User Interface for the R Package TIMP. *Journal of Statistical Software* **49**, 1–22 (2012).
4. Bensasson, R. & Land, E. J. Triplet-triplet extinction coefficients via energy transfer. *Trans. Faraday Soc.* **67**, 1904–1915 (1971).
5. Amand, B. & Bensasson, R. Determination of triplet quantum yields by laser flash absorption spectroscopy. *Chemical Physics Letters* **34**, 44–48 (1975).
6. Compton, R. H., Grattan, K. T. V. & Morrow, T. Extinction coefficients and quantum yields for triplet—triplet absorption using laser flash photolysis. *Journal of Photochemistry* **14**, 61–66 (1980).
7. Nielsen, B. R., Jørgensen, K. & Skibsted, L. H. Triplet—triplet extinction coefficients, rate constants of triplet decay and rate constant of anthracene triplet sensitization by laser flash photolysis of astaxanthin, β-carotene, canthaxanthin and zeaxanthin in deaerated toluene at 298 K. *Journal of Photochemistry and Photobiology A: Chemistry* **112**, 127–133 (1998).
8. Walker, B. J., Musser, A. J., Beljonne, D. & Friend, R. H. Singlet exciton fission in solution. *Nature Chemistry* **5**, 1019–1024 (2013).

9. Eaton, S. W. *et al.* Singlet Exciton Fission in Polycrystalline Thin Films of a Slip-Stacked Perylenediimide. *J. Am. Chem. Soc.* **135**, 14701–14712 (2013).
10. Zirzlmeier, J. *et al.* Singlet fission in pentacene dimers. *PNAS* **112**, 5325–5330 (2015).
11. Sanders, S. N. *et al.* Quantitative Intramolecular Singlet Fission in Bipentacenes. *J. Am. Chem. Soc.* **137**, 8965–8972 (2015).
12. Kumarasamy, E. *et al.* Tuning Singlet Fission in π-Bridge-π Chromophores. *J. Am. Chem. Soc.* **139**, 12488–12494 (2017).
13. Hetzer, C. *et al.* Chromophore Multiplication To Enable Exciton Delocalization and Triplet Diffusion Following Singlet Fission in Tetrameric Pentacene. *Angewandte Chemie International Edition* **58**, 15263–15267 (2019).
14. Korovina, N. V., Pompetti, N. F. & Johnson, J. C. Lessons from intramolecular singlet fission with covalently bound chromophores. *J. Chem. Phys.* **152**, 040904 (2020).